OPTIMAL ROBUST CONTROLLER DESIGN FOR VOLTAGE SOURCE INVERTERS IN MICROGRIDS

BY

WASIU OLAOTI SULAIMON
A Thesis Presented to the
DEANSHIP OF GRADUATE STUDIES

KING FAHD UNIVERSITY OF PETROLEUM & MINERALS

DHAHRAN, SAUDI ARABIA

In Partial Fulfillment of the
Requirements for the Degree of

MASTER OF SCIENCE

In

ELECTRICAL ENGINEERING

DECEMBER 2017

KING FAHD UNIVERSITY OF PETROLEUM & MINERALS

DHAHRAN- 31261, SAUDI ARABIA

DEANSHIP OF GRADUATE STUDIES

This thesis, written by **Wasiu Olaoti Sulaimon** under the direction his thesis advisor and approved by his thesis committee, has been presented and accepted by the Dean of Graduate Studies, in partial fulfillment of the requirements for the degree of **MASTER OF SCIENCE IN ELECTRICAL ENGINEERING**.

Dr. Mohammad Ali Abido
(Advisor)

Dr. Ali Ahmed Al-Shaikhi
Department Chairman

Dr. Ibrahim Mohamed El-Amin
(Member)

Dr. Salam A. Zummo
Dean of Graduate Studies

Dr. Ibrahim Omar Habiballah
(Member)

Date

Dedicated to my late mother HAOLAT ABDUL-AZEEZ

ACKNOWLEDGMENTS

Allah deserves all praise. His grace is pivotal to the successful completion of this thesis work.

My profound appreciation goes to my esteemed advisor, Professor Abido, for his patience with me and golden suggestions that pave a smooth way in this Journey. Also, I would like to thank him for a special moment where I benefited from his generosity and understanding.

I would like to thank all my family members, especially my wife, Shittu Bilikisu Temitope, for their moral supports and prayers throughout this journey. Also, to the Nigerian community at KFUPM, I acknowledged their good association and brotherhood.

My alloyed appreciation to all my colleagues at the Power System Research Group for their effort and support when the chips are down.

Lastly, I thank the Kingdom of Saudi Arabia for this scholarship opportunity at KFUPM. May Allah never cease to shower his blessings on the Kingdom.

TABLE OF CONTENTS

LIST OF TABLES

LIST OF FIGURES

LIST OF ABBREVIATIONS

AC   :   Alternating Current

AD   :   Active Damping

DC   :   Direct Current

DER   :   Distributed Energy Resources

DG   :   Distributed Generation

DSM   :   Demand Side Management

FC MPC   :   Finite Control Set Model Predictive Control

FFT   :   Fast Fourier Transform

LMI   :   Linear Matrix Inequality

MPC   :   Model Predictive Control

PD   :   Passive Damping

PID   :   Proportional Integral Derivative

PLL   :   Phase Locked Loop

PR   :   Proportional Resonant

PSO   :   Particle Swarm Optimization

PWM   :   Pulse Width Modulation

PV	:	Photovoltaic
RES	:	Renewable Energy Sources
RTDS	:	Real Time Digital Simulator
RTHIL	:	Real Time Hardware in Loop
SMC	:	Sliding Mode Control
THD	:	Total Harmonic Distortion
UPS	:	Uninterruptible Power Supply
VSI	:	Voltage Source Inverter

ABSTRACT

Full Name : [Wasiu Olaoti Sulaimon]

Thesis Title : [Optimal Robust Controller Design for Voltage Source Inverters in Microgrids]

Major Field : [Electrical Engineering]

Date of Degree : [December 2017]

The evolution of the conventional power systems to a smart grid system is of special interest to the global power system community with the influx of renewable energy resources (RES) as one of the drivers. A dimension of the smart grid proposed to address the problem of RES integration is the microgrid. The successful integration of these RES requires effective control of power electronics interface needed for power processing such as voltage source inverters(VSI). Therefore, the objective of this work is to device an optimal robust controller for a VSI that can effectively control a microgrid microsource both in the standalone and grid-connected mode of the microgrid. In this work, an optimal robust H_2 norm controller is proposed. This control strategy is easy to implement, accommodate system uncertainties and external disturbances in the controller design. In the two operating modes, the system is modelled in such a way that H_2 norm of the closed loop transfer function is optimized to ensure the system's stability and immunity to external perturbations. Also, the control strategy is observer-based to limit the number measured signals needed for feedback action. The proposed controller is verified via simulation and experimentation. The controller performed satisfactorily in terms of output tracking, decoupling capability, robustness and immunity to exogenous disturbances. Aside that, the controller shows better performance compared to reported literature.

ملخص الرسالة

الاسم الكامل: واسيوا الاوتي سليمان

عنوان الرسالة: تصميم المتحكمات المتينية المثالية لقلابات مصدر الجهد في الشبكات الصغيرة

التخصص: الهندسة الكهربائية

تاريخ الدرجة العلمية: ديسمبر/2017

تطور أنظمة الطاقة التقليدية إلى نظام الشبكة الذكية هو ذات أهمية خاصة للمجتمع نظام الطاقة العالمي مع تدفق موارد الطاقة المتجددة (RES) باعتبارها واحدة من السائقين. وهناك بعد من الشبكة الذكية المقترحة لمعالجة مشكلة تكامل RES هي الشبكة الصغيرة. يتطلب التكامل الناجح لهذه RES السيطرة الفعالة على واجهة الالكترونيات الطاقة اللازمة لمعالجة الطاقة مثل محولات مصدر الجهد (VSI). ولذلك، فإن الهدف من هذا العمل هو جهاز وحدة تحكم قوية الأمثل ل VSI التي يمكن السيطرة على نحو فعال ميكروسورس ميكروغريد على حد سواء في وضع مستقل ووضع متصل بالشبكة من الشبكة الصغيرة. في هذا العمل، ويقترح وحدة تحكم معيار H_2 الأمثل الأمثل. ومن السهل تنفيذ استراتيجية التحكم هذه، واستيعاب الشكوك في النظام والاضطرابات الخارجية في تصميم وحدة التحكم. في أوضاع التشغيل اثنين، على غرار النظام في مثل هذه الطريقة التي H_2 معيار وظيفة نقل حلقة مغلقة هو الأمثل لضمان استقرار النظام والحصانة للاضطرابات الخارجية. أيضا، واستراتيجية التحكم هو القائم على المراقب للحد من عدد الإشارات المقاسة اللازمة للعمل ردود الفعل. يتم التحقق من وحدة تحكم المقترحة عن طريق المحاكاة والتجريب. أداء وحدة التحكم بشكل مرض من حيث تتبع الناتج، والقدرة على فك الارتباط، والمتانة والحصانة للاضطرابات الخارجية. وبصرف النظر عن ذلك، وحدة تحكم يظهر أداء أفضل بالمقارنة مع الأدب ذكرت.

CHAPTER 1

INTRODUCTION

1.1   Motivation

With the proliferation of DG/DER, their integration into the grid has been a focal point of research. Individual integration and control of several DG and DER are difficult. From this motivation, the idea of microgrid was conceived as a potential solution to accommodate several DG and DER and integrate them into the grid [1],[2].

Microgrid is a small-scale version of the conventional grid that bridges the gap between generation and distribution. In other words, it is a miniaturized power system that accommodates DER, DG and loads in coordinated fashion to ensure reliable supply of electricity [3]. This reliability can be achieved in two different operating modes i.e. grid-connected and autonomous modes [4],[5].

Regardless of the mode the microgrid operates, coordination of the components to achieve a secured and reliable level of operation requires systematic control strategies. Irrespective of the control methods adopted, they are all centered on the power electronic converters in consideration. In other words, whatever goal we want to achieve with microgrid requires manipulating power converters interfaced with the DG and DER [6].

Successful integration of DER units in microgrid is not an easy task. DER integration poses operational bottlenecks that need to be considered when designing the control system in

order to maintain the desired level of reliability and security. Among the most relevant challenges are the bidirectional capabilities of the distribution system, low inertia and error in modeling assumptions.

The microgrid control system should have desirable attributes [7]. These include:

- Proper tracking and regulation of output currents and voltages of the DER units and the loads.

- Ability to share power among DER units in the case of power imbalance while restraining voltage and frequency deviations within limits.

- Proper demand side management (DSM) mechanisms to have control over the load.

- Appropriate economic dispatch of the DER units to decrease operating cost and augments profits.

- Seamless and smooth transition between grid-connected and autonomous modes of operation.

1.2 Problem Statement

An optimal robust controller based on H_2 norm minimization via linear matrix inequality (LMI) optimization will be designed for a single DG or DER with LC filter in a microgrid for both autonomous and grid-connected modes. In the autonomous mode, as well as for uninterruptible power supply (UPS) applications, the control objective is to regulate the microgrid voltage within the specified safe limit irrespective of the current drawn by the load as well as unforeseen changes in the system parameters that could be manifested in the inductor and capacitor filter nominal values. As for the grid-connected mode, the

control objective is to inject pure sinusoidal current to the grid and conform with the active and reactive power demand by the grid regardless of the uncertainties posed by the grid coupling resistance and inductances. To verify the effectiveness of these controllers, simulations will be carried out as well as experimental validations. For the simulation, MATLAB/SIMULINK environment will be adopted while Real-time hardware-in-loop (RTHIL) experimental setup involving real time digital simulator (RTDS) and dSPACE DS1103 board will be used to garner experimental results.

1.3   Thesis Objective

The objectives of this thesis are enumerated below:

1. To develop an optimal robust controller via LMI optimization for VSI in UPS applications, standalone and grid-connected modes in microgrids operation.

2. Evaluate, under different operating scenarios of the system, its performance and effectivity.

3. To validate the simulation results experimentally via RTHIL experimental test using RTDS and implementing the controller on dSPACE DS1103 board to ascertain the effectiveness of the proposed controller.

4. To conduct a detailed analysis of the performance of the controller in comparison to conventional controllers and similar robust controllers.

5. To analyze the THD of the current injected to the grid to ensure compliance with practical standard.

1.4   Contribution

The major contributions of this work are listed as follow:

1. Design of a novel discrete time optimal H_2 norm robust controller for VSI in the standalone mode of the Microgrid and UPS applications.

2. Design of another discrete-time optimal robust H_2 norm controller for VSI in the grid-connected mode of the microgrid.

3. Simulation and experimental validation of the optimality and robustness of these proposed controllers.

1.5   Thesis Organization

The rest of the chapters begins with Chapter 2. Chapter 2 gives a sufficient detail account of supporting literatures about this thesis. It begins with a brief background on the concept of Microgrids and VSI control. Then, it concludes with information about previous controllers that has designed for the same system under study. Chapter 3 introduces the design of a novel discrete time optimal robust H_2 control for a VSI connected to a microgrid in the standalone mode that can as well be implemented for UPS applications. In Chapter 4, another novel discrete time optimal robust H_2 norm controller is designed as a current control strategy for a single VSI connected to a microgrid in the grid-connected mode. Chapter 5 and Chapter 6 presents the results of the simulation and experimental work for islanded and grid-connected modes. Lastly, Chapter 7 concludes this thesis and recommendation for future improvement.

CHAPTER 2

LITERATURE REVIEW

Microgrid is understood to be a technological solution to the integration of DER units to the conventional grid and serve as an electricity life-line to geographical locations remote from the grid [8],[9]. This in turn, according to most research work, addresses the issue of climate change to some extent, and reduces depleting limited energy resources and environmental degradation [10]. However, the idea of integrating DGs and DERs into the microgrid requires sophisticated approach when controlling the microgrid [11]. This is due to the evident fact that microgrid's paradigm is somewhat distinguishable from the conventional power system norm. Similarly, the control of microgrid with dissimilar micro-sources is usually achieved via power electronics interfaces [12].

2.1   Microgrid Control

In power system control, centralized and decentralized approaches are the main approaches regarding architecture. In the centralized approach, a central controller gathers information of all participating units and makes decision on how best they should operate. The main demerit of this approach is that it needs extensive communication [13]. While local measurement does not seem to be appropriate in decentralized control in the case of strong coupling between DER units [7][14].

Each of these approaches has its merits and demerits. An alternative approach aside the two methods is to make use of the advantage of the two approaches. This is generally known as hierarchical approach [15]. This control scheme consists of three levels i.e.

5

primary, secondary and tertiary control schemes. What distinguishes them is time frame of operation the speed of response [16],[17]. Also, infrastructure requirements play another dividing factor. Due to the limited scope of this research, only the primary control would be examined in detail.

The primary control scheme is the basic level in the control scheme having the quickest response due to direct measurements of their control variables and requires no communication for making control decisions. Due to this fast response and speed requirement, islanding detection, power sharing scheme and output voltage control are usually included in this scheme [18],[19].

Most of the objectives of the primary control are carried out by the voltage source inverters (VSI). The main VSI controllers are responsible for power sharing among DG units and the inverter output control [20]. The DG power sharing controller is responsible for the sufficient allotment of real and reactive powers in the microgrid in the case of power mismatches. This is usually implemented by mimicking the droop characteristics of synchronous generators [21],[22]. Whereas, the task of the inverter output control is to regulate and stabilize output voltages and currents. The structures usually have outer loop for voltage stabilization and current regulation using inner loop [23].

2.2   Voltage Source Inverters Control

Power electronics converters have proliferated in the actualization of microgrid control and operation [24]. Therefore, a key success in the control of microgrid lies in the coordination of the power electronics interfaced DER units. These converters come in different topology and structure due to the type of micro-sources involved. For instance, DC-type micro-

sources like solar PV, energy storage unit and fuel cells require DC-AC power converter interfaces. Some micro-sources with output of varying frequencies like wind turbines and some controllable loads require the use of AC-AC interfaces [25]. These are possible if the microgrid of reference is an AC microgrid.

Due to the scope of this work, primary control will be our focus in this work. In a precise term, this control mainly includes inverter control and the power sharing control [7]. These two control techniques ensure a reliable and improved system performance, voltage and frequency regulation and proper DG units power sharing. Moreover, the inverter control will be given much attention in this work.

The inverter control usually referred to as the VSI control is responsible for achieving satisfactory performance in terms of regulation and disturbance rejections [26]. Much research efforts have been expended in designing suitable controllers to achieve the objectives of the inverter control. These controllers have merits and drawbacks; however, researches are on-going to overcome these short comings.

2.3   VSI Control for Standalone Mode and UPS Applications

The design effective controllers for distributed generations with DC-AC voltage source inverter interface such as uninterruptible power supply (UPS) and grid forming inverters in microgrid applications is still a subject of interest especially in the industrial communities [27]. This is because of the ubiquity of critical and sensitive loads in these industrial environments such as data centers, communication systems, and medical support equipment in hospitals etc. [28]. Therefore, it is expedient to design controllers of high

performance for UPS to ensure well-regulated and less distorted output voltage regardless of the kind of load connected to their terminals [29].

In this regard, quite many control strategy have been devised to achieve the objectives especially due to the rapid development of digital signal processors (DSP). Among the classical discrete linear controllers for UPS, deadbeat control proved to have fast transient response and short settling time within few sampling instants [30]. Conversely, it is reported to be sensitive to changes in system parameters and requires additional control subsystems to mitigate the problem posed by uncertainties, disturbances, and parameter mismatches. Also, the popular proportional-integral-differential (PID) controllers also offer good transient response and regulation, which is usually implemented in multi-loop fashion [30],[31]. However, in real situations, the coupling between the inner and outer loop dynamics with unmodeled dynamics might yield poor tracking and dynamic response. In an effort to improve on the PID using the same multi-loop structure, the parameters of the PID are optimized using particle swarm optimization (PSO) and considering the deviation in system parameters as constraints in the computation [32]. Also, decoupling and compensating terms are added to the multi-loop loop structure to improve the dynamic performance of the controller designed in the d-q reference frame [33]. However, the coupling was only reduced but not eliminated.

Another addition to the list is the repetitive controllers. They have the capability to reduce periodic distortions introduced by unknown periodic disturbances [34],[35],[36].Also, However, in the advent of aperiodic disturbances, they are slow in dynamics and require large memory [37],[38]. Although, a cost effective repetitive controller was proposed in [39]. Also, a novel design method tapping into the time advance unit of repetitive

controllers for a single phase inverter for UPS was developed to enhance overall system stability [40].

Aside the control strategies above, nonlinear controllers are also employed in UPS applications. Among them is sliding mode controllers (SMC). They are robust and easy to implement [41]. The phenomenon of chattering is usually the demerit of these controllers, however, considerable effort to reduce this drawback was proposed in [42],[43]. Adaptive control is also part of the control strategy used for UPS applications. The controllers are undoubtedly robust and respond well to system uncertainties without information about the structure of the system [44]. A combination of proportional resonant PR controller and SMC was also proposed in [45] to achieve stability and robustness. The main issue with these controllers is that computational complexity is high.

Recently, model predictive control is being used also for UPS applications especially finite control set model predictive control (FC MPC). FC MPC utilizes the advantage of the finite states of the inverter and model the associating system to make prediction of the output via simple optimization algorithm [46],[47],[48]. Because of this, they are very simple in implementation and efficient in computation [49]. However, a detailed analysis of the system stability and robustness is still undocumented.

Furthermore, robust control schemes based on linear matrix inequalities via convex optimization are also employed in several occasions for UPS applications and DG in autonomous microgrids. A multi-loop H-infinity control design immune to disturbance rejection and uncertainty in the system load impedance was proposed in [29]. Similarly, an LMI optimization approach for offset tracking was also presented where the system is

modeled with uncertainties assumed to be present in LC filter parameters and load resistance [50],[51]. An optimal observer based control having feedback term for stability and tracking is used with a compensating term needed to cater for system uncertainties was proposed in [52].

2.4 VSI Control in Grid-connected Mode

VSI employed for microgrids connected to the grid are referred to as grid feeding converters. In this case, the microgrid voltage and frequency are supported by the grid and the associated control is synchronized with the grid [53]. Their main purpose is to wheel power to the main grid [20]. The transfer of power to the grid is usually achieved through the technique of current control which eventually translates to active and reactive power demand [54],[55].

Aside feeding the grid, the VSI should be able to fulfill at least, to a required standard, power quality and voltage variation issues. For the power quality case, the THD of the current supplied to the grid should conform to the standard in [56],[57]. Also, the DG with VSI interface must be able to ride through variations in the grid voltage especially in the case of wind turbine integration [58],[59].

Therefore, whichever control strategy that is adopted, the VSI should be able to supply less distorted three-phase currents regardless of the grid voltage variations.

2.4.1 Damping Control Techniques

In sequel to the above discussion, voltage generated by the VSI are usually of high harmonic contents due to the PWM technique. Therefore, it is customary to append filter structures to VSI output terminal to eliminate unwanted harmonics [60],[61]. For the L

filter structure, it poses the problem of size due to large inductance value and switching frequency which later result to power losses [62]. As for the higher order filter structure like L, LC, LCL, and other variants, they tend to be smaller in size and have good power quality. However, the problem of resonance is an issue. Therefore, the controller design should be able to damp resonance associated with these structures[63]. Hence, a complex controller design is inevitable.

There are two major ways to damp the resonance triggered by complex filter structure with VSI in the grid-connected mode. The earliest method is the passive approach. This is usually implemented in a simple fashion by adding passive elements to the filter structure[32],[63],[64].However, the damping resistors constitute power losses and there is a poor rejection of high order harmonics. The second approach is the active damping control. This method employs control algorithms implemented in DSP controller to reshape the current control strategy [65],[66] .

2.4.2 Robust Active Damping Control Techniques

There have been many research works directed to active damping control strategy for VSI with complex filter structure connected to the grid [67]. The conventional approach is the vector control strategy usually employed in the case of L filters. They utilize the PI controllers and modified version to compensate for only dominant poles of the d-q axis using the zeroes of the PI controllers. However, in the case of LCL filters, this approach cannot mitigate the effect of uncompensated poles of the controlled system [68],[69]. A clever approach using state feedback with PI to compensate for all poles of the system using an appropriate pole placement technique [70],[71]. Also, a hybrid approach which is

a mix of AD and PD with capacitor filter current feedback was proposed in [72] to guarantee strong robustness, stability and harmonic rejection.

To tackle this issue of damping resonance, some robust control strategies based on robust full state and partial state feedback have been adopted. Although, they are robust and have satisfactory performances but there is no economic use of sensors[62],[73].Similarly, a robust pole location using LMI approach was also proposed in [74]. However, it suffers the same drawback of using the whole states for feedback as stated earlier. To solve the problem of using the whole states for feedback, a robust PLL scheme using open loop filtering technique via LMI optimization was proposed in [75]. Also, a H_∞ synthesis procedure was used to shape the input admittance of the VSI filter structure connected to the grid [76]. In addition, a novel full state observation with extended state observer using only inverter current feedback was also proposed in [77]. Another recent approach to tackle stability issue of VSI LCL interface was using H_∞ design approach via LMI optimization [78]. This method guarantees decoupling of the d-q control channels and responds well to system parameters' variation.

2.4.3 Knowledge Gaps

With knowledge drawn from different active damping control strategies for VSI tied to the grid and in the islanded mode with LCL interface, the following areas could be improved:

- Developing an exhaustive simple robust controller capable of considering the system parameters' uncertainties and external disturbances

- Improving on the already established results in terms of performances such as robustness, decoupling ability and dynamic transient behaviour.

CHAPTER 3

PROPOSED CONTROLLER: ISLANDED MODE

In this section, an optimal robust controller will be designed for a VSI in the standalone mode. In other words, the concept of optimal control and robust control are merged together to achieve results of desired performances and realization of a controlled system immune to intrinsic and extrinsic disturbances. Since the microgrid voltage is no longer supported by the grid in the autonomous mode, the overall objective of the control task is to ensure the microgrid terminal voltage stay within acceptable limits.

3.1 System Description
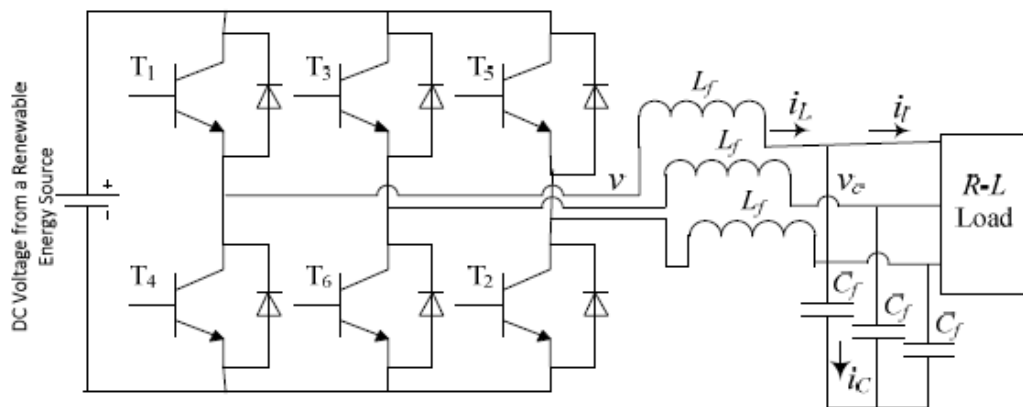
Figure 3-1: Schematic for VSI in Standalone Mode [51]

Fig. 3-1 shows a simplified schematic of a VSI microgrid system operating in the standalone mode. The DC power source is arbitrary. It could be from an AC rectifier

interfacing conventional AC power source like microturbines or DC power source from

renewable energy source like Solar. It is assumed that DC link is balanced and controlled.

Hence, it is not included in the schematic. The DC source is interfaced with the rest of the

system via 2-level inverter bridge using conventional PWM to generate firing pulses to

actuate the Inverter. The Inverter output is also coupled to the local load through an LC

filter structure to mitigate the effect of harmonics. Thereafter, the control objective is to

ensure that microgrid output voltage and the operating frequency are compliant with the

reference signals irrespective of increase in the load. This type of modelling is well

described in [79].

3.2   System Modelling
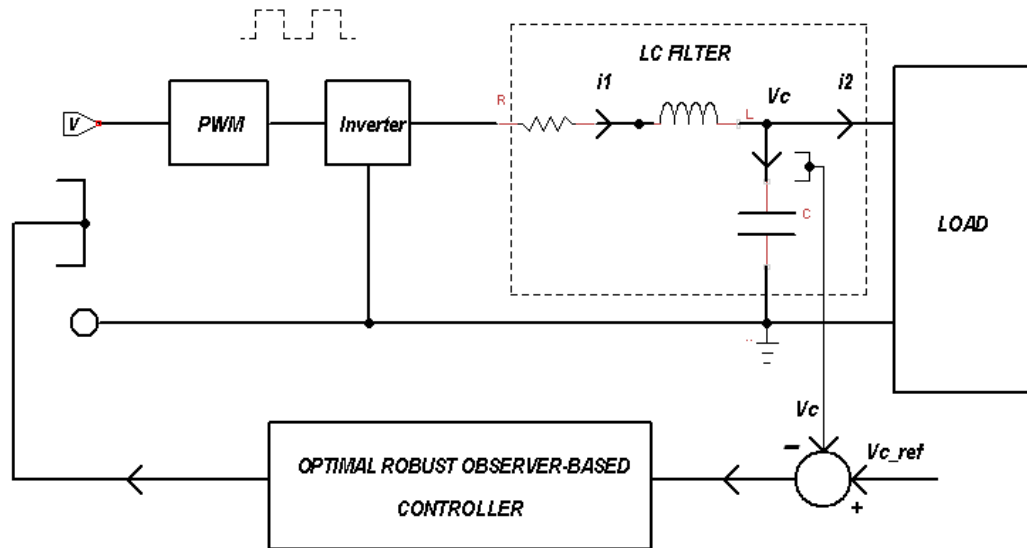
Figure 3-2: Control scheme representation of the system

The system in Fig. 3-2 shows the single-phase representation of the actual three-phase UPS system. The primary source to the inverter could be a conventional power source or renewable energy source like solar photovoltaic (PV). The inverter is fed by the pulsed width modulator (PWM) whose input is supplied by the optimal robust observer-based controller implemented in a digital controller prototype. To suppress the harmonics induced by the PWM, an LC filter is interfaced with the inverter, which is then connected to the load. The load is considered a black box. That is, it could be a linear or nonlinear load. Therefore, the objective of the control design is to make sure the output voltage is well regulated irrespective of the type of load connected to the system.

3.2.1 Mathematical Model

From Fig. 3-2, with the assumption that the switching frequency of the inverter is much greater than the system frequency, the linear time invariant (LTI) representation in space vector format can be written as:

$$\begin{bmatrix} \dfrac{di_1(t)}{dt} \\ \dfrac{dv_c(t)}{dt} \end{bmatrix} = \begin{bmatrix} \dfrac{-r_f}{L_f} & -\dfrac{1}{L_f} \\ \dfrac{1}{C_f} & 0 \end{bmatrix} \begin{bmatrix} i_1(t) \\ v_c(t) \end{bmatrix} + \begin{bmatrix} \dfrac{1}{Lf} \\ 0 \end{bmatrix} v(t) + \begin{bmatrix} 0 \\ -\dfrac{1}{C_f} \end{bmatrix} i_2(t) \qquad (3.1)$$

$$v_c(t) = \begin{bmatrix} 0 & 1 \end{bmatrix} \begin{bmatrix} i_1(t) \\ v_c(t) \end{bmatrix}$$

where $i_1(t), v_c(t), v(t),$ and $i_2(t)$ are the phasor representation of the inductor current, the voltage across the capacitor, the inverter input voltage, and the current drawn by the load

respectively. Also, r_f, L_f, and C_f are the filter parasitic resistance in the inductor, inductance, and capacitance respectively.

3.2.2 Discrete Time Modelling

From the space vector representation of the dynamics of the system as described in (3.1), the dynamics of the system in the synchronous reference frame can easily be expressed as:

$$\frac{dx_{dq}(t)}{dt} = A_c x_{dq}(t) + B_c u_{dq}(t) + E_c d_{dq}(t) \tag{3.2}$$

$$y_{dq}(t) = C_c x_{dq}(t) + D_c u_{dq}(t)$$

where the continuous state variables $x_{dq}(t) = \begin{bmatrix} i_{1d}(t) & i_{2d}(t) & v_{cd}(t) & v_{cq}(t) \end{bmatrix}^T$ are defined in the d-q reference frame as the inductor current, voltage across the capacitor and the grid inductor current respectively. The input and output of the system in the d-q frame are $u_{dq}(t) = \begin{bmatrix} v_d(t) & v_q(t) \end{bmatrix}^T$ and $y_{dq}(t) = \begin{bmatrix} v_{cd}(t) & v_{cq}(t) \end{bmatrix}^T$ respectively. Also, the disturbance signal is represented as $d_{dq}(t) = \begin{bmatrix} i_{2d}(t) & i_{2q}(t) \end{bmatrix}^T$. The system matrices after transforming (3.1) to the d-q reference frame are derived as:

$$A_c = \begin{bmatrix} -\dfrac{r_f}{L_f} & w & \dfrac{-1}{L_f} & 0 \\ -w & \dfrac{-r_f}{L_f} & 0 & \dfrac{-1}{L_f} \\ \dfrac{1}{C_f} & 0 & 0 & 0 \\ 0 & \dfrac{1}{C_f} & 0 & 0 \end{bmatrix}, B = \begin{bmatrix} \dfrac{1}{L_f} & 0 \\ 0 & \dfrac{1}{L_f} \\ 0 & 0 \\ 0 & 0 \end{bmatrix}, E_c = \begin{bmatrix} 0 & 0 \\ 0 & 0 \\ \dfrac{-1}{C_f} & 0 \\ 0 & \dfrac{-1}{C_f} \end{bmatrix} \tag{3.3}$$

$$C_c = \begin{bmatrix} 0 & 0 & 1 & 0 \\ 0 & 0 & 0 & 1 \end{bmatrix}, \quad D_c = \begin{bmatrix} 0 & 0 \\ 0 & 0 \end{bmatrix}$$

Since the actual controller is to be implemented as a digital controller, it is more appropriate that the control design be carried out in discrete time. With an appropriate sampling time, the discrete time representation of the model in the synchronous reference frame can be expressed as:

$$x_{dq}[k+1] = A_d x_{dq}[k] + B_d u_{dq}[k] + E_d d_{dq}[k] \tag{3.4}$$

$$y_{dq}[k] = C_d x_{dq}(k) + D_d u_{dq}[k]$$

where the discrete state variables $x_{dq}[k]$, the output $y_{dq}[k]$, and the input signals $u_{dq}[k]$ are the discrete counterpart of the same variable previously defined. With a sufficient sampling interval, T, the discrete state space system matrices are computed in the conventional manner of discretization as:

$$A_d = e^{A_c T}, \ B_d = \left(\int_0^T e^{A_c \tau} d\tau \right) B, \ C_d = C_c, \ D_d = D_c \tag{3.5}$$

3.3 Control Problem Formulation

The objective of the controller is to ensure that the output voltage tracks the set-point voltage as required. To achieve a satisfactory steady state error response, (3.4) can be modified as both regulation and tracking problem immune to external disturbances.

For the tracking problem, an error variable is introduced as:

$$e_{dq}[k] = y_{ref}[k] - y_{dq}[k] \tag{3.6}$$

Using recursion and the defined output equation, with $y_{ref}[k+1] - y_{ref}[k] = 0$

$$e_{dq}[k+1] = e_{dq}[k] - C_d\left(x_{dq}[k+1] - x_{dq}[k]\right) - D_d\left(u_{dq}[k+1] - u_{dq}[k]\right) \tag{3.7}$$

Next, new discrete state variable $z_{dq}[k]$ and a new input signal $v_{dq}[k]$ are defined and expressed as:

$$z_{dq}[k] = x_{dq}[k+1] - x_{dq}[k] \tag{3.8}$$

$$v_{dq}[k] = u_{dq}[k+1] - u_{dq}[k] \tag{3.9}$$

Also, from (3.8), a new difference equation of the system dynamics can be derived recursively as:

$$z_{dq}[k+1] = x_{dq}[k+2] - x_{dq}[k+1] \tag{3.10}$$

$$z_{dq}[k+1] = A_d\left(x_{dq}[k+1] - x_{dq}[k]\right) + B_d\left(u_{dq}[k+1] - u_{dq}[k]\right) + E_d\left(d_{dq}[k+1] - d_{dq}[k]\right) \tag{3.11}$$

$$z_{dq}[k+1] = A_d z_{dq}[k] + B_d v_{dq}[k] + E_d w_{dq}[k] \tag{3.12}$$

By combining (3.7) and (3.12), the overall state space model of the system can be written as:

$$\begin{bmatrix} z_{dq}[k+1] \\ e_{dq}[k+1] \end{bmatrix} = \begin{bmatrix} A_d & 0 \\ -C_d & I \end{bmatrix} \begin{bmatrix} z_{dq}[k] \\ e_{dq}[k] \end{bmatrix} + \begin{bmatrix} B_d \\ -D_d \end{bmatrix} v_{dq}[k] + \begin{bmatrix} E_d \\ 0 \end{bmatrix} w_{dq}[k] \tag{3.13}$$

In a compact form, the state space can be expressed as:

18

$$\eta_{dq}[k+1] = \tilde{A}\eta_{dq}[k] + \tilde{B}v_{dq}[k] + \tilde{E}w_{dq}[k] \qquad (3.14)$$

$$e_{dq}[k] = \tilde{C}\eta_{dq}[k] + \tilde{D}w_{dq}[k] \qquad (3.15)$$

where the new system matrices are further defined as:

$$\tilde{A} = \begin{bmatrix} A_d & 0 \\ -C_d & I \end{bmatrix}, \; \tilde{B} = \begin{bmatrix} B_d \\ 0 \end{bmatrix}, \; \tilde{E} = \begin{bmatrix} E_d \\ 0 \end{bmatrix}, \; \tilde{C} = \begin{bmatrix} 0 & I \end{bmatrix}, \; \tilde{D} = \begin{bmatrix} 0 & 0 \\ 0 & 0 \end{bmatrix}$$

Finally, the original state space model of the actual system has been transformed to a type amenable for the intended controller design. In other words, the task of the controller will be to design a state feedback to regulate the states to zero and while reducing the effect of the external disturbances on the output. This will be achieved by designing tunable H_2 norm controller implemented using LMI convex approach.

3.4   Proposed H_2 Controller Design

3.4.1 Mathematical Model

Redefining (3.14) and (3.15) as:

$$\eta_{dq}[k+1] = \tilde{A}_c\eta_{dq}[k] + \tilde{E}w_{dq}[k] \qquad (3.16)$$

$$e_{dq}[k] = \tilde{C}\eta_{dq}[k] + \tilde{D}w_{dq}[k] \qquad (3.17)$$

where the system input $v_{dq}[k] = -K_{opt}\eta_{dq}[k]$ and the closed loop matrices are defined as

$\tilde{A}_c = \tilde{A} - \tilde{B}K_{opt}$ and K_{opt} is the state feedback controller gain.

Now, the system transfer function from the external input to the output can be written as:

$$G(z) = \tilde{C}\left(zI - \tilde{A}_c\right)^{-1} \tilde{E} + \tilde{D} \tag{3.18}$$

Therefore, the conventional H_2-norm minimization of the effect of the external input on the output of the system can be expressed as:

$$\|G(z)\|_{H_2} = \sqrt{trace\left(\tilde{E}^T Q \tilde{E}\right)} \tag{3.19}$$

where $\tilde{Q}$, a positive definite matrix, is the solution of the matrix algebraic equation in (3.19) as defined below.

$$-Q + \tilde{A}_c{}^T Q \tilde{A}_c + \tilde{C}^T \tilde{C} = 0 \tag{3.20}$$

Suppose $\|G(z)\|_{H_2} < \gamma$, H_2-norm minimization can be restated in the form of a matrix inequality as:

$$trace\left(\tilde{E}^T Q \tilde{E}\right) < \gamma^2 \tag{3.21}$$

$$-Q + \tilde{A}_c{}^T Q \tilde{A}_c + \tilde{C}^T \tilde{C} < 0 \tag{3.22}$$

where γ is a positive real number.

Theorem: For the system in (3.16) and (3.17), the H_2-norm of the transfer function is less than γ which invariably guarantees stability and regulation if there exist $X > 0, Y > 0$, and $Z > 0$ such that the following conditions are satisfied.

$$trace(Z) < \gamma^2 \tag{3.23}$$

20

$$\begin{bmatrix} Z & \tilde{E}^T \\ \tilde{E} & X \end{bmatrix} > 0 \qquad (3.24)$$

$$\begin{bmatrix} X & X\tilde{A}^T - Y^T\tilde{B}^T & X\tilde{C}^T \\ \tilde{A}X - \tilde{B}Y & X & 0 \\ CX & 0 & I \end{bmatrix} > 0 \qquad (3.25)$$

Proof: Starting from the first condition in (3.21), a positive definite matrix Z is defined such that $Z > \tilde{E}^T Q\tilde{E}$. If $trace(Z) < \gamma$, then $trace(\tilde{E}^T Q\tilde{E}) < \gamma^2$. This implies:

$$Z - \tilde{E}^T Q\tilde{E} > 0 \qquad (3.26)$$

Using the Schur's complement, the above Equation can be rewritten as:

$$\begin{bmatrix} Z & \tilde{E}^T \\ \tilde{E} & X \end{bmatrix} > 0 \qquad (3.27)$$

where $X = Q^{-1}$.

Similarly, the second condition in (3.22) which is obviously not amenable to convex optimization can be written as:

$$Q - \begin{bmatrix} \tilde{A}_c^T Q & \tilde{C}^T \end{bmatrix} \begin{bmatrix} Q^{-1} & 0 \\ 0 & I \end{bmatrix} \begin{bmatrix} Q\tilde{A}_c \\ \tilde{C} \end{bmatrix} > 0 \qquad (3.28)$$

Next, the Schur's complement principle can be employed to rewrite (3.28) as:

$$\begin{bmatrix} Q & \tilde{A}_c^T Q & \tilde{C}^T \\ Q\tilde{A}_c & Q & 0 \\ \tilde{C} & 0 & I \end{bmatrix} > 0 \qquad (3.29)$$

Since (3.29) is not a linear matrix inequality due to the terms containing the closed loop matrix, this Equation can be pre- and post-multiplied by an appropriate positive definite matrix via the congruence relation as:

$$
\begin{bmatrix} Q^{-1} & 0 & 0 \\ 0 & Q^{-1} & 0 \\ 0 & 0 & I \end{bmatrix} \begin{bmatrix} Q & \tilde{A}_c^T Q & \tilde{C}^T \\ Q\tilde{A}_c & Q & 0 \\ \tilde{C} & 0 & I \end{bmatrix} \begin{bmatrix} Q^{-1} & 0 & 0 \\ 0 & Q^{-1} & 0 \\ 0 & 0 & I \end{bmatrix}^T > 0 \tag{3.30}
$$

Consequently, (30) yields:

$$
\begin{bmatrix} X & X\tilde{A}_c & X\tilde{C}^T \\ \tilde{A}_c X & X & 0 \\ \tilde{C}X & 0 & I \end{bmatrix} > 0 \tag{3.31}
$$

Substituting for the $\tilde{A}_c$ to get a more explicit expression, this yields;

$$
\begin{bmatrix} X & X\tilde{A}^T - Y^T\tilde{B}^T & X\tilde{C}^T \\ \tilde{A}X - \tilde{B}Y & X & 0 \\ \tilde{C}X & 0 & I \end{bmatrix} > 0 \tag{3.32}
$$

where $Y = K_{opt}X$ and this completes the proof.

3.4.2 Controller Implementation

From the controller design approach, the output of the controller is not the actual input required by the system. It is necessary to transform the output of the controller in terms of the required states of the system. In this regard, from (3.16), the auxiliary controller output is

$$v_{dq}[k] = \begin{bmatrix} -K_1 & -K_2 \end{bmatrix} \begin{bmatrix} z_{dq}[k] \\ e_{dq}[k] \end{bmatrix} \tag{3.33}$$

where $K_{opt} = \begin{bmatrix} K_1 & K_2 \end{bmatrix}$. Hence, (3.33) in the Z-domain can be written as

$$V_{dq}(z) = -K_1 Z_{dq}(z) - K_2 E_{dq}(z) \tag{3.34}$$

where $V_{dq}(z), Z_{dq}(z)$, and $E_{dq}(z)$ represent the Z-transform of $v_{dq}[k]$, $z_{dq}[k]$, and $e_{dq}[k]$, respectively.

From (3.8), the relationship between $v_{dq}[k]$ and $u_{dq}[k]$ in the frequency Z-domain can be written as:

$$V_{dq}(z) = (z-1)U_{dq}(z) \tag{3.35}$$

Likewise, for the states of the system, we have

$$Z_{dq}(z) = (z-1)X_{dq}(z) \tag{3.36}$$

Therefore, substituting for $V_{dq}(z)$ and $Z_{dq}(z)$ in (3.33) yields;

$$U_{dq}(z) = -K_1 X_{dq}(z) - K_2 \left(\frac{1}{z-1} \right) E_{dq}(z) \tag{3.37}$$

3.5   Reduced Order Observer Design

In this section, a reduced order observer will be designed to generate the estimate of the required states needed for state feedback. In this case, all the states will be estimated but excluding the states that has direct relationship with the output. With the assumption that $x \in \Re^n$ and $y \in \Re^m$ where the output signals can be measured with a sensor directly,

23

hence, the reduced-order observer will be of the order $n - m$. Therefore, the actual state space model can be reformulated in (3.14) without loss of generality as:

$$\begin{bmatrix} x_1[k+1] \\ y[k+1] \end{bmatrix} = \begin{bmatrix} A_{11} & A_{12} \\ A_{21} & A_{22} \end{bmatrix} \begin{bmatrix} x_1[k] \\ y[k] \end{bmatrix} + \begin{bmatrix} B_1 \\ B_2 \end{bmatrix} u[k] + \begin{bmatrix} E_1 \\ E_2 \end{bmatrix} d[k] \tag{3.38}$$

$$y[k] = \begin{bmatrix} 0 & I \end{bmatrix} \begin{bmatrix} x_1[k] \\ y[k] \end{bmatrix}$$

where $x_1[k]$, $y[k]$, $u[k]$, and $d[k]$ represent $z_{dq}[k]$, $e_{dq}[k]$, $w_{dq}[k]$, and $v_{dq}[k]$, respectively. Also, the system matrices can be represented as follows:

$$\begin{bmatrix} A_{11} & A_{12} \\ A_{21} & A_{22} \end{bmatrix} = \begin{bmatrix} A_d & 0 \\ -C_d & I \end{bmatrix}, \quad \begin{bmatrix} B_1 \\ B_2 \end{bmatrix} = \begin{bmatrix} B_d \\ 0 \end{bmatrix}, \quad \begin{bmatrix} E_1 \\ E_2 \end{bmatrix} = \begin{bmatrix} E_d \\ 0 \end{bmatrix} \tag{3.39}$$

For the unmeasured portion of the state space model above, the state is thus given by

$$x_1[k+1] = A_{11}x_1[k] + A_{12}y[k] + B_1u[k] + E_1d[k] \tag{3.40}$$

The dynamics of the second subsystem can be rewritten as

$$y[k+1] - A_{22}y[k] - B_2u[k] - E_2d[k] = A_{21}x_1[k] \tag{3.41}$$

and the RHS of the above equation will be regarded as the output signal of (3.39). Therefore, the estimate of (3.39) can be formulated as:

$$\hat{x}_1[k+1] = (A_{11} + LA_{12})\hat{x}_1[k] + A_{12}y[k] + B_1u[k] - L(y[k+1] - A_{22}y[k] - B_2u[k]) \tag{3.42}$$

where L is the observer gain matrix to be designed.

24

The reduced-order state estimate defined above requires an advanced signal of the output i.e. $y[k+1]$ which is obviously not needed. To overcome this difficulty, it is customary to define an intermediate estimate signal to get rid of this term. This is defined as:

$$\hat{\eta}[k] = \hat{x}_1[k] + Ly[k] \tag{3.43}$$

Then, the final expression of the intermediate signal can be written as:

$$\hat{\eta}[k+1] = (A_{11} + LA_{12})\hat{\eta}[k] + (A_{12} + LA_{22} - (A_{11} + LA_{21})L)y[k] + (B_1 + LB_2)u[k] \tag{3.44}$$

The feedback controller designed with the estimated states can now be expressed as:

$$u[k] = -[K_1 \quad K_2] \begin{bmatrix} \hat{x}_1[k] \\ y[k] \end{bmatrix} \tag{3.45}$$

which implies;

$$v_{dq}[k] = [-K_1 \quad -K_2] \begin{bmatrix} \hat{z}_{dq}[k] \\ e_{dq}[k] \end{bmatrix} \tag{3.46}$$

In the Z-domain, from (3.36), the control law can be written as:

$$U_{dq}(z) = -K_1 \hat{X}_{dq}(z) - K_2 \left(\frac{1}{z-1} \right) E_{dq}(z) \tag{3.47}$$

where the relationship between $\hat{X}_{dq}(z)$ and $\hat{Z}_{dq}(z)$ is already expressed in (3.35). However, $\hat{X}_{dq}(z)$ is not directly estimated as discussed above. Hence, from (3.42), the equivalent estimate can be written as:

25

$$\hat{X}_{dq}(z) = \frac{z}{1-z} \Lambda_{dq}(z) - L \frac{E_{dq}(z)}{1-z} \tag{3.48}$$

where $\Lambda_{dq}(z)$ is the Z-transform of $\hat{\eta}[k]$. Hence, the final expression for the control law in the Z-domain can be written as:

$$U_{dq}(z) = -K_1 \left(\frac{z}{1-z} \right) \Lambda_{dq}(z) + (K_1 L - K_2) \left(\frac{1}{1-z} \right) E_{dq}(z) \tag{3.49}$$

Finally, in a compact form, the dynamic output feedback controller utilizing reduced order observer can be written in state space form based on the information in (3.43) and (3.48) as

$$\hat{\eta}_{dq}[k+1] = A \hat{\eta}_{dq}[k] + B e_{dq}[k] \tag{3.50}$$

$$u_{dq}[k] = C \hat{\eta}[k] + D e_{dq}[k]$$

where

$$A = A_{11} + L A_{21} - (B_1 + L B_2) K_1, \quad B = (B_1 + L B_2)(K_1 L - K_2) + (A_{12} + L A_{22}) - (A_{11} + L A_{21}) L$$

$$C = -K_1, \quad D = K_1 L - K_2 \tag{3.51}$$

3.6 Conclusion

In this section, a single microsource in the standalone mode operation of a microgrid is taken as a case study. The system is modelled in such a way that the loads connected to the systems are represented as disturbances. Thereafter, an observer-based H_2 robust controller

is designed to guarantee the stability of the system while also minimizing the effect of the

addition of loads on the output voltage of the microgrid.

CHAPTER 4

PROPOSED CONTROLLER: GRID-CONNECTED

MODE

In this chapter, an optimal robust controller is designed for VSI microgrid system connected to the grid. In this case, the microgrid voltage and frequency are supported by the grid. Therefore, the task is to feed into the grid satisfactorily minimally distorted sinusoidal current according to the demands from the grid. The first section in this chapter deals with modelling of the system with uncertainties. In the second section, the design of an optimal robust controller based on H_2 convex optimization approach. Finally, based on the conventional principle of separation in classical control, a reduced-order observer will be designed to get the estimate of unmeasured states needed for feedback control.

4.1   Description of the System

The VSI microgrid system, operating in the grid-connected mode, is like the system described in Section 3.1 except with the interface to the grid. The microgrid system is connected to grid via a coupling resistance and inductance. In some cases, it could be a transformer. Also, the microgrid voltage is now being supported by the grid. Hence, a phase locked loop (PLL) is required to help with the synchronization. The control objective is current controlled strategy where current is being fed to grid which translates to active and reactive power demand.
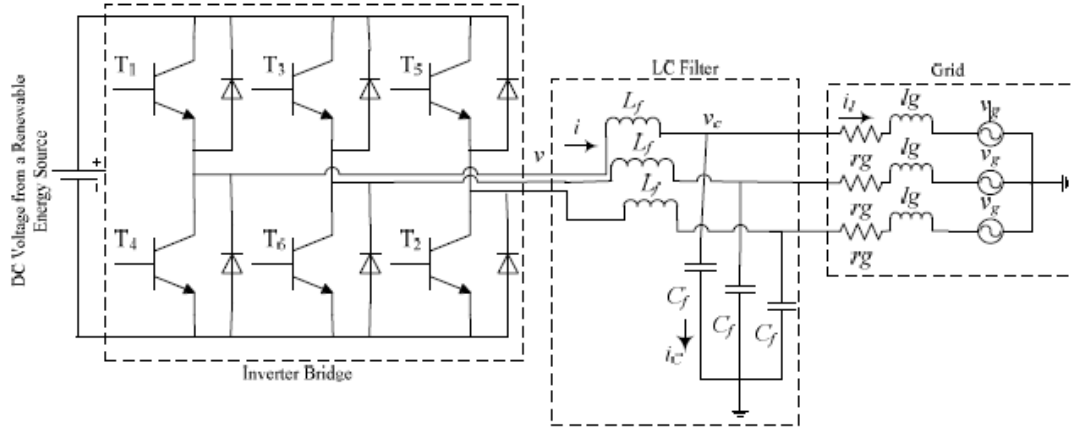
Figure 4-1: Grid-connected Microgrid VSI system LC filter structure

4.2 Modelling of the VSI with LC Filter Structure

Following the same procedure as in Chapter 3, the space vector representation of the dynamics of the system in state space can be expressed as

$$
\frac{d}{dt}\begin{bmatrix} i_1(t) \\ v_c(t) \\ i_2(t) \end{bmatrix} = \begin{bmatrix} \dfrac{-R_f}{L_f} & \dfrac{-1}{L_f} & 0 \\ \dfrac{1}{C_f} & 0 & \dfrac{-1}{C_f} \\ 0 & \dfrac{1}{L_g} & \dfrac{-R_g}{L_g} \end{bmatrix}\begin{bmatrix} i_1(t) \\ v_c(t) \\ i_2(t) \end{bmatrix} + \begin{bmatrix} \dfrac{1}{L_f} \\ 0 \\ 0 \end{bmatrix} v(t) + \begin{bmatrix} 0 \\ 0 \\ \dfrac{-1}{L_g} \end{bmatrix} v_g(t) \tag{4.1}
$$

$$
i_2(t) = \begin{bmatrix} 0 & 0 & 1 \end{bmatrix}\begin{bmatrix} i_1(t) \\ v_c(t) \\ i_2(t) \end{bmatrix} \tag{4.2}
$$

where the space vector quantities corresponding to the filter-inductor current, the microgrid voltage, the current fed to the grid, and the grid voltage are depicted as $i_1(t)$, $v_c(t)$, $i_2(t)$ and $v_g(t)$ respectively. Also, the physical parameters R_f, L_f, C_f, R_g and L_g are the parasitic resistance of the filter inductor, inductance of the filter inductor, filter capacitance, grid coupling resistance and inductance respectively. Also, Equation 3.1 represents the space vector dynamics of the system in the state space form while Equation 3.2 represents the overall objective which is to ensure the current fed to the grid is less distorted and tracks sufficiently the demand from the grid.

4.2.1 Discrete Time Model in DQ Frame

From the space vector representation of the dynamics of the system as described in (4.1), the dynamics of the system in the synchronous reference frame can easily be expressed as

$$\dot{x}_{dq}(t) = Ax_{dq}(t) + Bu_{dq}(t) + Ed_{dq}(t) \tag{4.3}$$

$$y_{dq}(t) = Cx_{dq}(t) + Du_{dq}(t) \tag{4.4}$$

where the continuous state variables $x_{dq}(t) = \begin{bmatrix} i_{1d}(t) & i_{2d}(t) & v_{cd}(t) & v_{cq}(t) & i_{2d}(t) & i_{2q}(t) \end{bmatrix}^T$ are defined in the d-q reference frame as the inductor current, voltage across the capacitor and the grid inductor current respectively. The input and output of the system in the d-q frame are $u_{dq}(t) = \begin{bmatrix} v_d(t) & v_q(t) \end{bmatrix}^T$ and $y_{dq}(t) = \begin{bmatrix} i_{2d}(t) & i_{2q}(t) \end{bmatrix}^T$ respectively. Also, the disturbance signal is represented as $d_{dq}(t) = \begin{bmatrix} v_{gd}(t) & v_{gq}(t) \end{bmatrix}^T$. The system matrices after the transformation in (4.3) and (4.4) are represented as

30

$$A = \begin{bmatrix} \dfrac{-R_f}{L_f} & w & \dfrac{-1}{L_f} & 0 & 0 & 0 \\[6pt] -w & \dfrac{-R_f}{L_f} & 0 & \dfrac{-1}{L_f} & 0 & 0 \\[6pt] \dfrac{1}{C_f} & 0 & 0 & w & \dfrac{-1}{C_f} & 0 \\[6pt] 0 & \dfrac{1}{C_f} & -w & 0 & 0 & \dfrac{-1}{C_f} \\[6pt] 0 & 0 & \dfrac{1}{L_g} & 0 & \dfrac{-R_g}{L_g} & w \\[6pt] 0 & 0 & 0 & \dfrac{1}{L_g} & -w & \dfrac{-R_g}{L_g} \end{bmatrix}, \quad B = \begin{bmatrix} \dfrac{1}{L_f} & 0 \\[6pt] 0 & \dfrac{1}{L_f} \\[6pt] 0 & 0 \\[6pt] 0 & 0 \\[6pt] 0 & 0 \\[6pt] 0 & 0 \end{bmatrix} \tag{4.5}$$

$$E = \begin{bmatrix} 0 & 0 \\ 0 & 0 \\ 0 & 0 \\ 0 & 0 \\ \dfrac{-1}{L_g} & 0 \\[6pt] 0 & \dfrac{-1}{L_g} \end{bmatrix} \quad C = \begin{bmatrix} 0 & 0 & 0 & 0 & 1 & 0 \\ 0 & 0 & 0 & 0 & 0 & 1 \end{bmatrix} \quad D = \begin{bmatrix} 0 & 0 \\ 0 & 0 \end{bmatrix}$$

Since the actual controller is to be implemented as a digital controller, it is more appropriate that the control design be carried out in discrete time. With an appropriate sampling time, the discrete time representation of the model in the synchronous reference frame can be represented as,

$$x_{dq}[k+1] = A_d x_{dq}[k] + B_d u_{dq}[k] + E_d d_{dq}[k] \tag{4.6}$$

$$y_{dq}[k] = C_d x_{dq}(k) + D_d u_{dq}[k] \tag{4.7}$$

where the discrete state variables $x_{dq}[k]$, the output $y_{dq}[k]$, the input signals $u_{dq}[k]$, and the disturbance signal $d_{dq}[k]$ are the discrete counterpart of the same variable previously defined. With a sufficient sampling interval T, the discrete state space system matrices are computed in the conventional manner of discretization as

$$A_d = e^{AT}, \; B_d = \left(\int_0^T e^{A\tau} d\tau \right) B, \; C_d = C, \; D_d = D, \; E_d = E \tag{4.8}$$

4.2.2 Modelling Uncertainties

It is not certain that system parameters' values will remain constant throughout the longevity of the microgrid operation. With this consideration, it is pertinent to ensure that the system remains stable and conformal to the objectives in the advent of changes in parameters. Unlike the VSI microgrid system in the standalone mode in Chapter 3, the uncertainty for this system is considered in the coupling resistance and inductance. Hence, with the uncertainties, the state space in (4.3) and (4.4) can be written as

$$\dot{x}_{dq}(t) = A(\theta)x_{dq}(t) + Bu_{dq}(t) + E(\theta)d_{dq}(t) \tag{4.9}$$

$$y_{dq}(t) = Cx_{dq}(t) + Du_{dq}(t) \tag{4.10}$$

where

32

$$A(\theta) = \begin{bmatrix} \dfrac{-r_f}{L_f} & w & \dfrac{-1}{L_f} & 0 & 0 & 0 \\[2mm] -w & \dfrac{-r_f}{L_f} & 0 & \dfrac{-1}{L_f} & 0 & 0 \\[2mm] \dfrac{1}{C_f} & 0 & 0 & w & \dfrac{-1}{C_f} & 0 \\[2mm] 0 & \dfrac{1}{C_f} & -w & 0 & 0 & \dfrac{-1}{C_f} \\[2mm] 0 & 0 & \dfrac{1}{\theta_1} & 0 & \dfrac{-\theta_2}{\theta_1} & w \\[2mm] 0 & 0 & 0 & \dfrac{1}{\theta_1} & -w & \dfrac{-\theta_2}{\theta_1} \end{bmatrix}, \quad E = \begin{bmatrix} 0 & 0 \\ 0 & 0 \\ 0 & 0 \\ 0 & 0 \\ \dfrac{-1}{\theta_1} & 0 \\ 0 & \dfrac{-1}{\theta_1} \end{bmatrix} \qquad (4.11)$$

where $A(\theta) \in$ **Convex Hull** $\{A_1, A_2, ..., A_\mu\}$ and $E(\theta) \in$ **Convex Hull** $\{E_1, E_2, ..., E_\delta\}$

The uncertain parameters can be expressed as convex combinations of the allowable range of their deviations. That is

$$\frac{1}{\theta_1} = \alpha_1 \frac{1}{\theta_1^{\min}} + \alpha_2 \frac{1}{\theta_1^{\max}} \qquad (4.12)$$

$$\theta_2 = \beta_1 \theta_2^{\min} + \beta_2 \theta_2^{\max} \qquad (4.13)$$

and

$$\alpha_1 + \alpha_2 = 1 \qquad (4.14)$$

$$\beta_1 + \beta_2 = 1 \qquad (4.15)$$

where α_1, α_1, β_1, and β_2 are real positive values in the range $[0,1]$ that determines the possible values of the uncertain parameters between the minimum and maximum values of the parameters

Therefore, $A(\theta)$ and $E(\theta)$ can be expressed as

$$A(\theta) = \alpha_1 \beta_1 A_1 + \alpha_1 \beta_2 A_2 + \alpha_2 \beta_1 A_3 + \alpha_2 \beta_2 A_4 \qquad (4.16)$$

$$E(\theta) = \alpha_1 E_1 + \alpha_2 E_2 \qquad (4.17)$$

and also,

$$A(\theta) = \sum_{k=1}^{4} \sigma_k A_k \qquad (4.18)$$

with the property that

$$\sum_{k=1}^{4} \sigma_k = 1 \qquad (4.19)$$

where

$$A_1 = \begin{bmatrix} \dfrac{-r_f}{L_f} & w & \dfrac{-1}{L_f} & 0 & 0 & 0 \\[2mm] -w & \dfrac{-r_f}{L_f} & 0 & \dfrac{-1}{L_f} & 0 & 0 \\[2mm] \dfrac{1}{C_f} & 0 & 0 & w & \dfrac{-1}{C_f} & 0 \\[2mm] 0 & \dfrac{1}{C_f} & -w & 0 & 0 & \dfrac{-1}{C_f} \\[2mm] 0 & 0 & \dfrac{1}{\theta_1^{\min}} & 0 & \dfrac{-\theta_2^{\min}}{\theta_1^{\min}} & w \\[2mm] 0 & 0 & 0 & \dfrac{1}{\theta_1^{\min}} & -w & \dfrac{-\theta_2^{\min}}{\theta_1^{\min}} \end{bmatrix}
\qquad
A_2 = \begin{bmatrix} \dfrac{-r_f}{L_f} & w & \dfrac{-1}{L_f} & 0 & 0 & 0 \\[2mm] -w & \dfrac{-r_f}{L_f} & 0 & \dfrac{-1}{L_f} & 0 & 0 \\[2mm] \dfrac{1}{C_f} & 0 & 0 & w & \dfrac{-1}{C_f} & 0 \\[2mm] 0 & \dfrac{1}{C_f} & -w & 0 & 0 & \dfrac{-1}{C_f} \\[2mm] 0 & 0 & \dfrac{1}{\theta_1^{\min}} & 0 & \dfrac{-\theta_2^{\max}}{\theta_1^{\min}} & w \\[2mm] 0 & 0 & 0 & \dfrac{1}{\theta_1^{\min}} & -w & \dfrac{-\theta_2^{\max}}{\theta_1^{\min}} \end{bmatrix}$$

34

$$A_3 = \begin{bmatrix} \dfrac{-r_f}{L_f} & w & \dfrac{-1}{L_f} & 0 & 0 & 0 \\[2ex] -w & \dfrac{-r_f}{L_f} & 0 & \dfrac{-1}{L_f} & 0 & 0 \\[2ex] \dfrac{1}{C_f} & 0 & 0 & w & \dfrac{-1}{C_f} & 0 \\[2ex] 0 & \dfrac{1}{C_f} & -w & 0 & 0 & \dfrac{-1}{C_f} \\[2ex] 0 & 0 & \dfrac{1}{\theta_1^{\,max}} & 0 & \dfrac{-\theta_2^{\,min}}{\theta_1^{\,max}} & w \\[2ex] 0 & 0 & 0 & \dfrac{1}{\theta_1^{\,max}} & -w & \dfrac{-\theta_2^{\,min}}{\theta_1^{\,max}} \end{bmatrix} \qquad A_4 = \begin{bmatrix} \dfrac{-r_f}{L_f} & w & \dfrac{-1}{L_f} & 0 & 0 & 0 \\[2ex] -w & \dfrac{-r_f}{L_f} & 0 & \dfrac{-1}{L_f} & 0 & 0 \\[2ex] \dfrac{1}{C_f} & 0 & 0 & w & \dfrac{-1}{C_f} & 0 \\[2ex] 0 & \dfrac{1}{C_f} & -w & 0 & 0 & \dfrac{-1}{C_f} \\[2ex] 0 & 0 & \dfrac{1}{\theta_1^{\,max}} & 0 & \dfrac{-\theta_2^{\,max}}{\theta_1^{\,max}} & w \\[2ex] 0 & 0 & 0 & \dfrac{1}{\theta_1^{\,max}} & -w & \dfrac{-\theta_2^{\,max}}{\theta_1^{\,max}} \end{bmatrix}$$

$$(4.20)$$

$$E_1 = \begin{bmatrix} 0 & 0 \\ 0 & 0 \\ 0 & 0 \\ 0 & 0 \\ \dfrac{-1}{\theta_1^{\,min}} & 0 \\[2ex] 0 & \dfrac{-1}{\theta_1^{\,min}} \end{bmatrix} , \quad E_2 = \begin{bmatrix} 0 & 0 \\ 0 & 0 \\ 0 & 0 \\ 0 & 0 \\ \dfrac{-1}{\theta_1^{\,max}} & 0 \\[2ex] 0 & \dfrac{-1}{\theta_1^{\,max}} \end{bmatrix}$$

and $(\theta_1, \theta_2) \in \Re$ are the uncertainties posed by the grid coupling resistance and inductance respectively.

4.3   Control Problem Formulation

Redefining (4.6) and (4.7) to model parameter uncertainties, the following Equation ensues

$$x_{dq}[k+1] = A_d(\theta)x_{dq}[k] + B_d u_{dq}[k] + E_d(\theta)d_{dq}[k] \tag{4.21}$$

$$y_{dq}[k] = C_d x_{dq}(k) + D_d u_{dq}[k] \tag{4.22}$$

The objective of the controller is to ensure that the output i.e. the current being fed to the grid tracks the set-point current on demand. Hence, the active and reactive power can be controlled via this method. To achieve a satisfactory steady error response, (4.21) and (4.22) can modified as both regulation and tracking problem immune to external disturbances.

For the tracking problem, an error variable is introduced as

$$e_{dq}[k] = y_{ref}[k] - y_{dq}[k] \tag{4.23}$$

Using recursion and the defined output equation,

$$e_{dq}[k+1] = e_{dq}[k] - C_d \left(x_{dq}[k+1] - x_{dq}[k] \right) - D_d \left(u_{dq}[k+1] - u_{dq}[k] \right) \tag{4.24}$$

Next, new discrete state variable $z_{dq}[k]$ and a new input signal $v_{dq}[k]$ are and defined expressed as

$$z_{dq}[k] = x_{dq}[k+1] - x_{dq}[k] \tag{4.25}$$

$$v_{dq}[k] = u_{dq}[k+1] - u_{dq}[k] \tag{4.26}$$

Also, from (4.25), a new difference equation of the system dynamics can be derived recursively as

$$z_{dq}[k+1] = x_{dq}[k+2] - x_{dq}[k+1] \tag{4.27}$$

$$z_{dq}[k+1] = A_d(\theta) \left(x_{dq}[k+1] - x_{dq}[k] \right) + B_d \left(u_{dq}[k+1] - u_{dq}[k] \right) + E_d \left(d_{dq}[k+1] - d_{dq}[k] \right) \tag{4.28}$$

$$z_{dq}[k+1] = A_d(\theta) z_{dq}[k] + B_d v_{dq}[k] + E_d(\theta) w_{dq}[k] \tag{4.29}$$

By combining (4.24) and (4.29), the overall state space model of the system can be written
as

$$
\begin{bmatrix} z_{dq}[k+1] \\ e_{dq}[k+1] \end{bmatrix} = \begin{bmatrix} A_d(\theta) & 0 \\ -C_d & I \end{bmatrix} \begin{bmatrix} z_{dq}[k] \\ e_{dq}[k] \end{bmatrix} + \begin{bmatrix} B_d \\ -D_d \end{bmatrix} v_{dq}[k] + \begin{bmatrix} E_d(\theta) \\ 0 \end{bmatrix} w_{dq}[k] \qquad (4.30)
$$

In a compact form, the state space can be expressed as

$$
\eta_{dq}[k+1] = \tilde{A}(\theta)\eta_{dq}[k] + \tilde{B}v_{dq}[k] + \tilde{E}(\theta)w_{dq}[k] \qquad (4.31)
$$

$$
e_{dq}[k] = \tilde{C}\eta_{dq}[k] + \tilde{D}w_{dq}[k] \qquad (4.32)
$$

where the new system matrices are further defined as

$$
\tilde{A}(\theta) = \begin{bmatrix} A_d(\theta) & 0 \\ -C_d & I \end{bmatrix}, \ \tilde{B} = \begin{bmatrix} B_d \\ 0 \end{bmatrix}, \ \tilde{E}(\theta) = \begin{bmatrix} E_d(\theta) \\ 0 \end{bmatrix}, \ \tilde{C} = \begin{bmatrix} 0 & I \end{bmatrix}, \ \tilde{D} = \begin{bmatrix} 0 & 0 \\ 0 & 0 \end{bmatrix} \qquad (4.33)
$$

Finally, the original state space model of the actual system has been transformed to a type
amenable for the intended controller design. In other words, the task of the controller will
be to design a state feedback to regulate the states to zero and while reducing the effect of
the external disturbances on the output. This will be achieved by designing tunable H_2-
norm controller implemented using convex approach.

4.4   Controller Design

The main task in this section is to design an observer-based robust optimal controller to
drive the system to the desired outcome. In other words, a reduced-order observer is
designed to estimate all the states needed for control except states linked directly to the

output. Afterwards, these estimated states are used as feedback with controller gain designed using H_2-norm minimization via LMI approach.
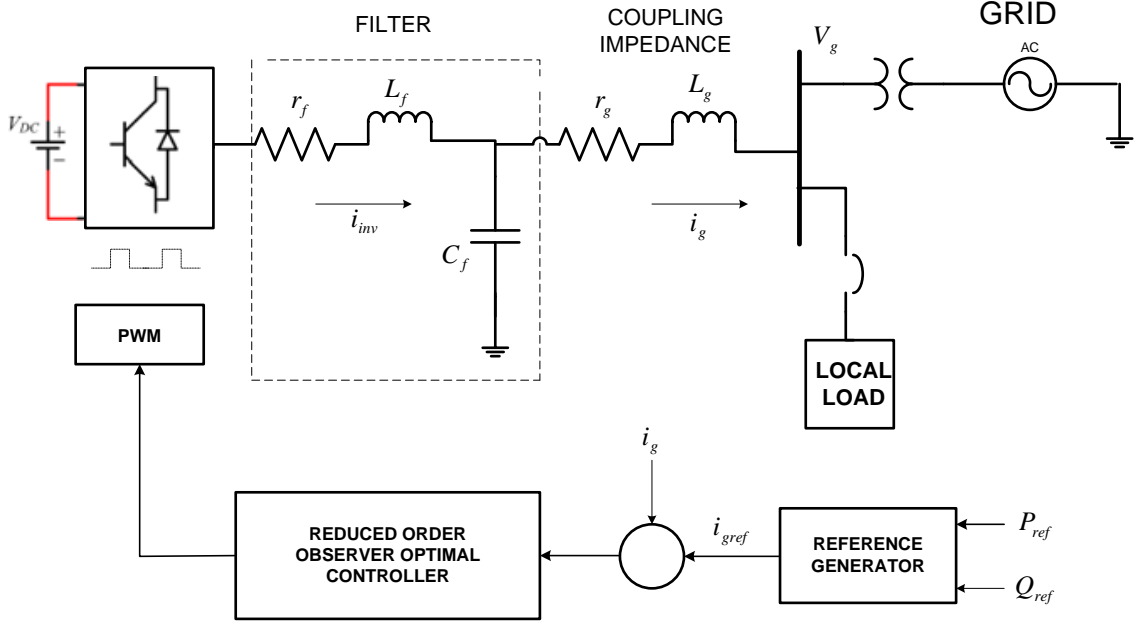

Figure 4-2 Block Diagram of the Control Procedure

4.4.1 Proposed Robust H-2 Norm Controller Design

The objective of this section is to determine a controller gain to stabilize the closed loop system while minimizing the effect of the disturbance on the output. In this case, we rewrite (4.31) to incorporate the controller gain and take the disturbance as the input to the system. That is

$$\eta_{dq}[k+1] = \tilde{A}_c(\theta)\eta_{dq}[k] + \tilde{E}(\theta)w_{dq}[k] \tag{4.34}$$

$$e_{dq}[k] = \tilde{C}\eta_{dq}[k] + \tilde{D}w_{dq}[k] \tag{4.35}$$

38

where the system input $v_{dq}[k] = -K_{opt}\eta_{dq}[k]$ and the closed loop matrices are defined as

$\tilde{A}_c(\theta) = \tilde{A}(\theta) - \tilde{B}K_{opt}$ with K_{opt} is the state feedback controller gain.

Now, the system transfer function from the external input to the output can be written as

$$G(z) = \tilde{C}\left(zI - \tilde{A}_c(\theta)\right)^{-1}\tilde{E}(\theta) + \tilde{D} \tag{4.36}$$

Therefore, the conventional H_2-norm minimization of the effect of the external input on the output of the system can be expressed as

$$\|G(z)\|_{H_2} = \sqrt{trace\left(\tilde{E}(\theta)^T Q\tilde{E}(\theta)\right)} \tag{4.37}$$

where $\tilde{Q}$, a positive definite matrix, is the solution of the matrix algebraic equation in (4.38) defined below as

$$-Q + \tilde{A}_c(\theta)^T Q\tilde{A}_c(\theta) + \tilde{C}^T\tilde{C} = 0 \tag{4.38}$$

Suppose the $\|G(z)\|_{H_2} < \gamma$, the H_2-norm minimization can be restated in the form of a matrix inequality as

$$trace\left(\tilde{E}(\theta)^T Q\tilde{E}(\theta)\right) < \gamma^2 \tag{4.39}$$

$$-Q + \tilde{A}_c(\theta)^T Q\tilde{A}_c(\theta) + \tilde{C}^T\tilde{C} < 0 \tag{4.40}$$

where γ is a positive real number.

Theorem: For the system in (4.34) and (4.35), the H_2-norm of the transfer function is less than γ which invariably guarantees stability and regulation if there exist $X > 0, Y > 0$ and $Z > 0$ such that the following conditions are satisfied

$$trace(Z) < \gamma^2 \tag{4.41}$$

$$\begin{bmatrix} Z & \tilde{E}_i^{\ T} \\ \tilde{E}_i & X \end{bmatrix} > 0 \ , \ 1 \leq i \leq 2 \tag{4.42}$$

$$\begin{bmatrix} X & X\tilde{A}_j^{\ T} - Y^T \tilde{B}^T & X\tilde{C}^T \\ \tilde{A}_j X - \tilde{B}Y & X & 0 \\ CX & 0 & I \end{bmatrix} > 0, \ 1 \leq j \leq 4 \tag{4.43}$$

Proof: Starting from the first condition in (4.39), a positive definite matrix Z is defined such that $Z > \tilde{E}(\theta)^T Q\tilde{E}(\theta)$. If $trace(Z) < \gamma$ then $trace\left(\tilde{E}(\theta)^T Q\tilde{E}(\theta)\right) < \gamma^2$. This implies that

$$Z - \tilde{E}(\theta)^T Q\tilde{E}(\theta) > 0 \tag{4.44}$$

Using the Schur's complement, the above Equation can be rewritten as

$$\begin{bmatrix} Z & \tilde{E}(\theta)^T \\ \tilde{E}(\theta) & X \end{bmatrix} > 0 \tag{4.45}$$

where $X = Q^{-1}$. Also, the above condition can be written explicitly in terms of the polytopes of $\tilde{E}(\theta)$ as

$$\begin{bmatrix} Z & \tilde{E}_i^T \\ \tilde{E}_i & X \end{bmatrix} > 0 \ , \ 1 \le i \le 2 \tag{4.46}$$

Similarly, the second condition in (4.40) which is obviously not amenable to convex optimization can be written as

$$Q - \begin{bmatrix} \tilde{A}_c(\theta)^T Q & \tilde{C}^T \end{bmatrix} \begin{bmatrix} Q^{-1} & 0 \\ 0 & I \end{bmatrix} \begin{bmatrix} Q\tilde{A}_c(\theta) \\ \tilde{C} \end{bmatrix} > 0 \tag{4.47}$$

Next, we employ the Schur's complement principle to rewrite (4.47) as

$$\begin{bmatrix} Q & \tilde{A}_c(\theta)^T Q & \tilde{C}^T \\ Q\tilde{A}_c(\theta) & Q & 0 \\ \tilde{C} & 0 & I \end{bmatrix} > 0 \tag{4.48}$$

Since (4.48) is not a linear matrix inequality due to the terms containing the closed loop matrix, we pre-multiply and post multiply this Equation by an appropriate positive definite matrix via the congruence relation as

$$\begin{bmatrix} Q^{-1} & 0 & 0 \\ 0 & Q^{-1} & 0 \\ 0 & 0 & I \end{bmatrix} \begin{bmatrix} Q & \tilde{A}_c(\theta)^T Q & \tilde{C}^T \\ Q\tilde{A}_c(\theta) & Q & 0 \\ \tilde{C} & 0 & I \end{bmatrix} \begin{bmatrix} Q^{-1} & 0 & 0 \\ 0 & Q^{-1} & 0 \\ 0 & 0 & I \end{bmatrix} > 0 \tag{4.49}$$

Consequently, (4.49) yields

$$\begin{bmatrix} X & X\tilde{A}_c(\theta) & X\tilde{C}^T \\ \tilde{A}_c(\theta)X & X & 0 \\ \tilde{C}X & 0 & I \end{bmatrix} > 0 \tag{4.50}$$

and substituting for the expression of $\tilde{A}_c(\theta)$ to get a more explicit expression, this yields

$$
\begin{bmatrix}
X & X\tilde{A}(\theta)^T - Y^T\tilde{B}^T & X\tilde{C}^T \\
\tilde{A}(\theta)X - \tilde{B}Y & X & 0 \\
\tilde{C}X & 0 & I
\end{bmatrix} > 0
\tag{4.51}
$$

where $Y = K_{opt}X$ and finally, the above condition can be written explicitly in terms of the

polytopes of $\tilde{A}(\theta)$ as

$$
\begin{bmatrix}
X & X\tilde{A}_j^T - Y^T\tilde{B}^T & X\tilde{C}^T \\
\tilde{A}_jX - \tilde{B}Y & X & 0 \\
CX & 0 & I
\end{bmatrix} > 0, \quad 1 \le j \le 4
\tag{4.52}
$$

This ends the proof.

4.4.2 Controller Implementation

From the controller design approach, the output of the controller is not the actual input

required by the system to function. It is necessary to transform the output of the controller

in terms of the required states of the system. In this regard, from (4.34), the auxiliary

controller output is

$$
v_{dq}[k] = \begin{bmatrix} -K_1 & -K_2 \end{bmatrix} \begin{bmatrix} z_{dq}[k] \\ e_{dq}[k] \end{bmatrix}
\tag{4.53}
$$

where $K_{opt} = \begin{bmatrix} K_1 & K_2 \end{bmatrix}$. Hence, (4.53) in the Z-domain can be written as

$$
V_{dq}(z) = -K_1 Z_{dq}(z) - K_2 E_{dq}(z)
\tag{4.54}
$$

where $V_{dq}(z), Z_{dq}(z)$, and $E_{dq}(z)$ represents the Z-transform of $v_{dq}[k], z_{dq}[k]$, and $e_{dq}[k]$

respectively.

From (4.26), the relationship between $v_{dq}[k]$ and $u_{dq}[k]$ in the frequency Z-domain can be written as

$$V_{dq}(z) = (z-1)U_{dq}(z) \qquad (4.55)$$

Likewise, for the states of the system, we have

$$Z_{dq}(z) = (z-1)X_{dq}(z) \qquad (4.56)$$

Therefore, substituting for $V_{dq}(z)$ and $Z_{dq}(z)$ in (4.53) yields

$$U_{dq}(z) = -K_1 X_{dq}(z) - K_2 \left(\frac{1}{z-1} \right) E_{dq}(z) \qquad (4.57)$$

4.5   Conclusion

In this section, an optimal robust controller for a grid-connected VSI in a microgrid that ensures active damping of the resonance inherent in the filter structure is proposed. The system is modelled as uncertain because of the inclusion of the grid coupling inductance and resistance in the modelling. Also, at the low voltage bus, nonlinear and linear loads could also be connected to the system. Then, an active damping H_2 control strategy is designed to damp resonance inherent in the LC filter circuit while supplying the grid with active and power demanded.

CHAPTER 5

RESULTS: STANDALONE VSI

In this chapter, the results of the simulations and experiments carried out on VSI that can be employed for both microgrid autonomous operation and UPS applications are presented. The cases studies span tracking test, robustness test and nonlinear load disturbance test.

5.1   System Schematics
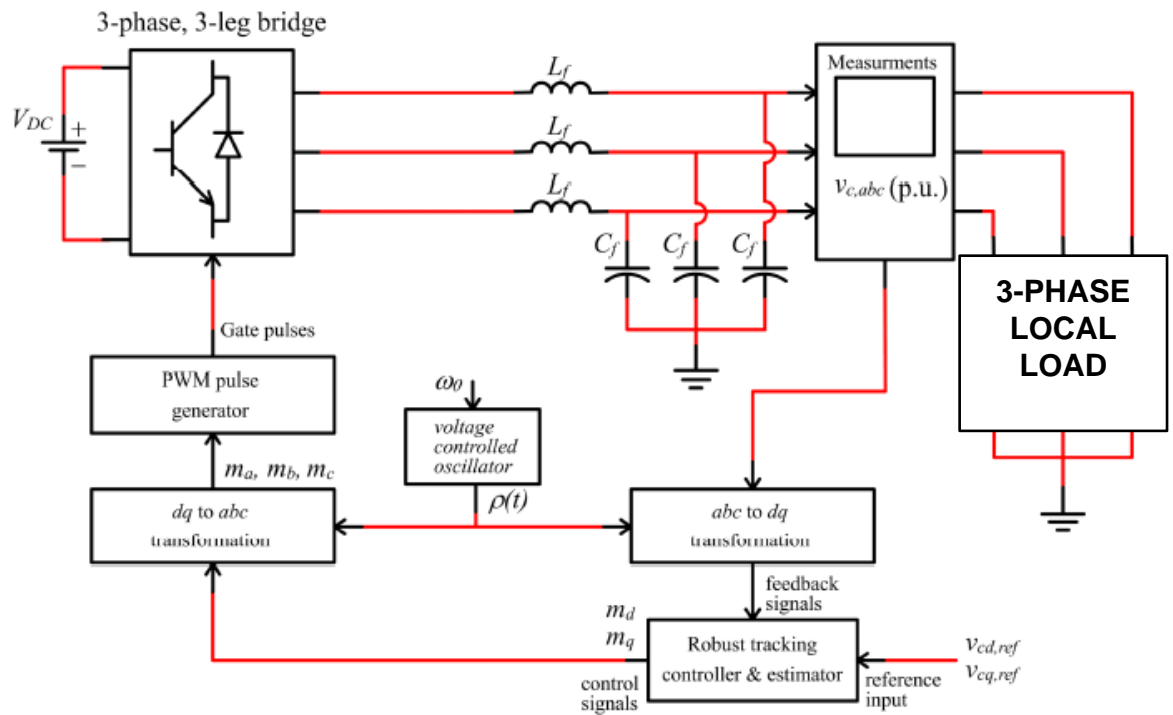
Figure 5-1: Schematic diagram for the VSI in the Islanded mode [80]

Fig. 5-1 shows a typical single power source unit with a voltage source inverter interface in a microgrid. For simplicity, power sources are represented by a constant voltage source with the assumption that the DC link capacitor voltage is well regulated. Therefore, the controller is not shown. Also, the 2-level inverter is fed with pulses from the PWM triggered by the robust optimal controller. The controller is implemented in the d-q reference frame, therefore, there is a necessity for signal transformation block from a-b-c frame to d-q frame and vice versa. The transformation units are synchronized with the system by adopting a local internal oscillator which acts like a pseudo PLL like the case in grid-connected mode. Because the output voltages from the inverter have large harmonic contents, it is customary to append L, LC, or LCL filter for harmonic suppression. In this work, an LC filter is used. It is preferable to L filter especially in terms of cost and size. However, for LC and LCL filters, there is usually a problem of resonance. Hence, the control design becomes more complex. As for the load, we will assume it to be RL linear load which could be interfaced to the system by an isolation transformer. If we assume the structure of the load to be unknown, then the load will be a black box while the current drawn from it will be modelled as disturbances.

5.2   System and Controller Parameters

The choice of system parameters for the simulation and experimental work are not arbitrary. Rather, they were chosen according to the parameters used in [81] which are shown in Table 5-1. The controller parameters after results of the convex optimization of (3.23) to (3.25) and observer gain from MATLAB using pole placement technique are shown in Table 5-2.

Table 1: System parameters

Parameters	Symbol	Value
DC Voltage	V_{dc}	480V
Frequency	f	60Hz
Filter Inductance	L_f	$0.8m$H
Filter Line Resistance	r_f	0.1Ω
Filter Capacitance	C_f	75μF
Nominal Load Resistance	R_0	5Ω
Nominal Line Inductance	L_0	$2m$H
Reference Output Voltage	V_c(RMS)	155.6 V
	$[V_{cdref} \quad V_{cqref}]$	[220 0] V
Sampling Time	T_s	2.5μs
Controller Sampling Time	T_{samp}	10μs

Table 2: Controller Parameters

Controller Parameters	Value
γ	1000
K_{opt}	$\begin{bmatrix} 184.0 & 0.11 & 68.14 & -0.071 & -1.43\times10^5 & 148.66 \\ -0.16 & 184.0 & 0.043 & 68.14 & -91.41 & -1.43\times10^5 \end{bmatrix}$
L	$\begin{bmatrix} -52.52 & -0.40 & -2.65 & -0.01 \\ -0.33 & -52.67 & -0.01 & -2.65 \end{bmatrix}^T$

5.3   Simulation Results

To ascertain the efficacy of the proposed controller, simulation tests for three different cases were carried out in MATLAB/SIMULINK as depicted in the schematic in Fig. 5-1. The system parameters used for the simulation cases are given in Table 5-1. Also, the controller gain parameters for the observer-based controller are also shown in Table 5-2. Theses parameters are also used for the experimental cases. Also, the whole SIMULINK blocks used for the simulations are shown in the appendix.

5.3.1   Tracking Results Simulation

The first simulation test is the tracking or regulation test. This test is carried out to confirm the tracking performance of the controller is the case of setpoint voltage change within the allowable deviations or any other form of disturbances that might cause a dip or sag in the output terminal voltage. For this case, the, the load is simulated as a resistive load of about 72kW which is about 150% more than the load for nominal parameters in Table 5-1 which is about 30kW.

Fig. 5-1 shows the tracking performance of the controller in the steady state. Within 0.045s and 0.06s, the output follows the reference adequately without any noticeable coupling with the q-axis. This is not the case for similar results in [81]. In Fig. 5-2, the three-phase voltage waveform and the load current drawn from the VSI system are also displayed.
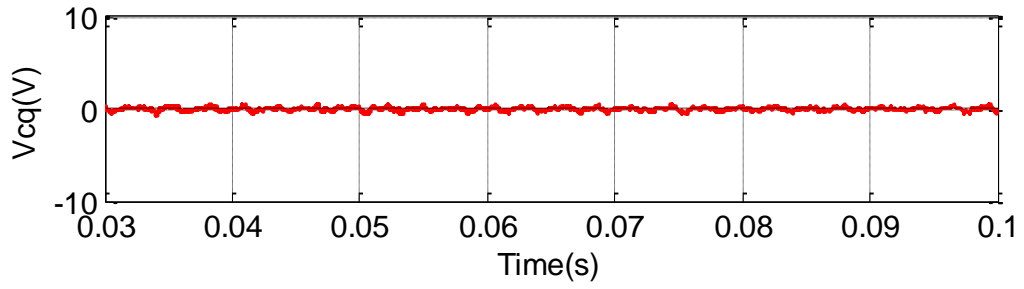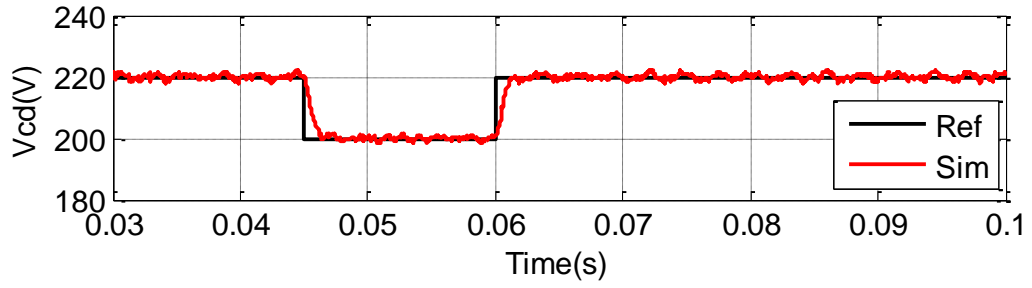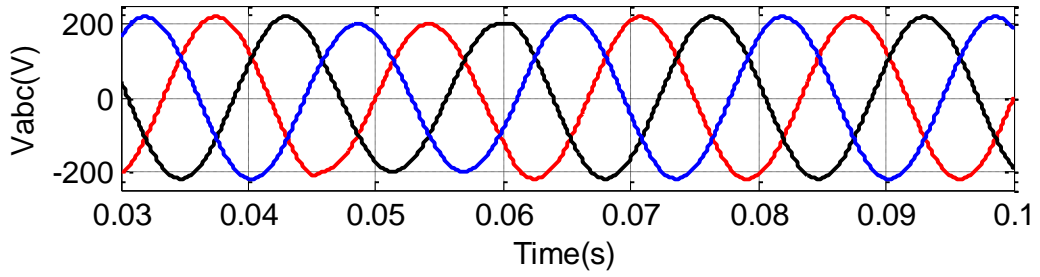
Figure 5-2: Output voltage tracking simulation test in d-q frame
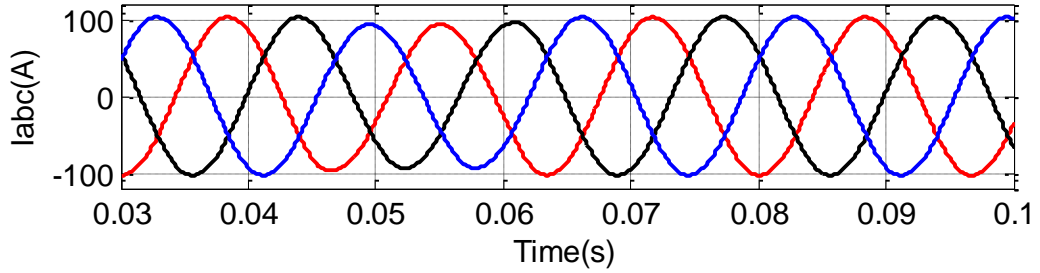
Figure 5-3: Output voltage and current in three-phase

5.3.2 Disturbance Simulation Test

The objective of this test is to examine the system's behaviour in the advent of sudden change in load. The nominal load is change by decreasing the nominal value of the load resistance and inductance by 25% at 0.03s and then restored back to the nominal values at 0.075s. Because of this, more load current is being drawn from the inverter and the output voltage stays relatively unperturbed. This is shown Fig. 5-4.

5.3.3 Simulation with Nonlinear Load

In this this test, the load is change to nonlinear load which is usually modelled as a combination of semiconductor devices and passive elements. For this simulation and the experimental cases, the structure of the nonlinear is shown Fig. 5-6. Regardless of the highly harmonic current drawn from the VSI system, the output voltage remains within bounds and less distorted as shown in Fig. 5-5.
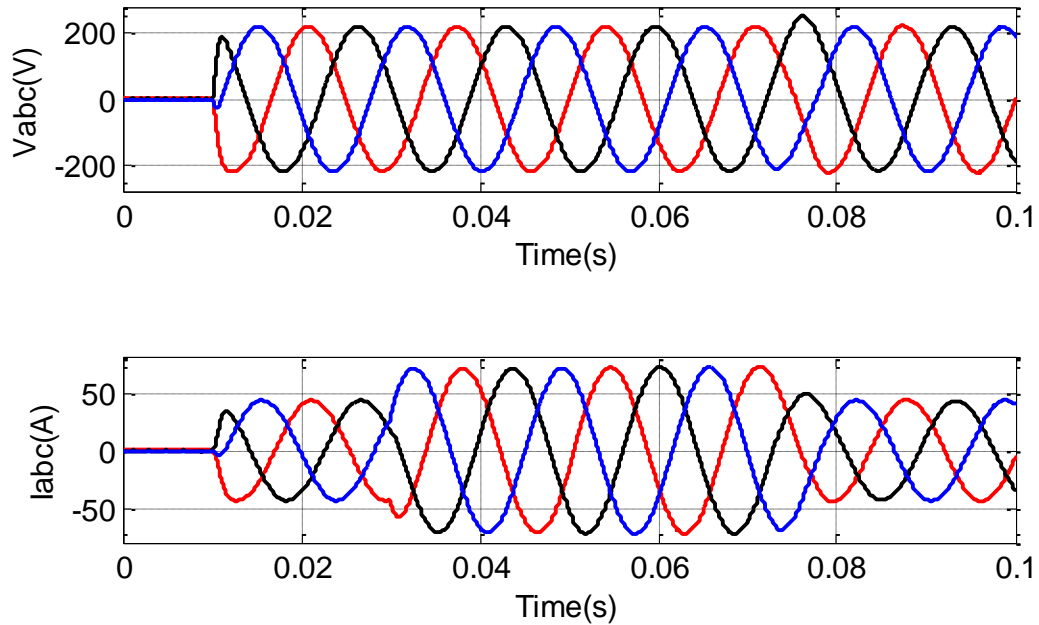
Figure 5-4: Output voltage and current in three-phase for disturbance test

49
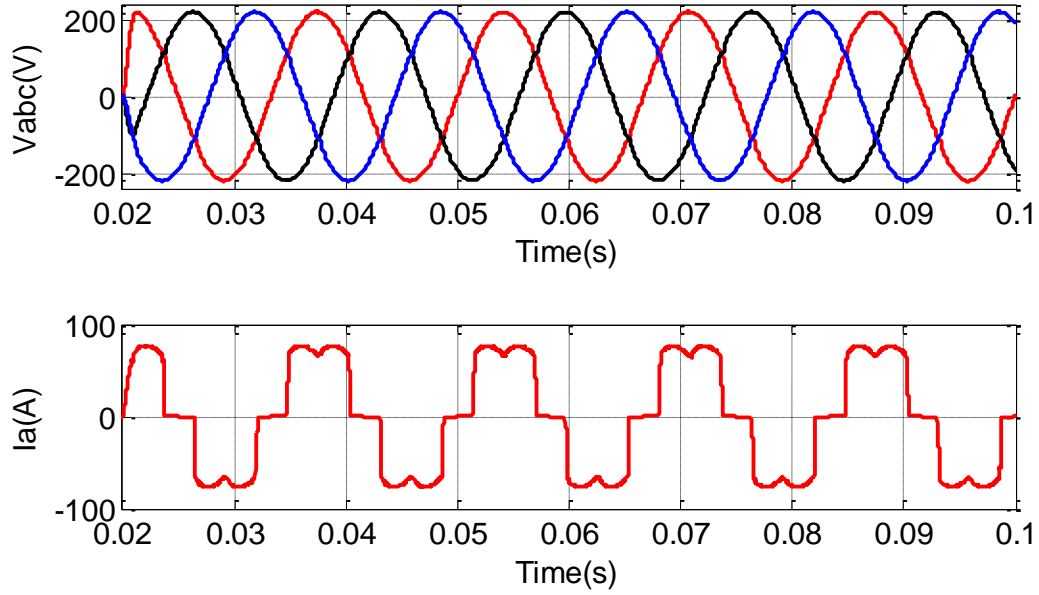
Figure 5-5: Output voltage and current in three-phase for nonlinear load test
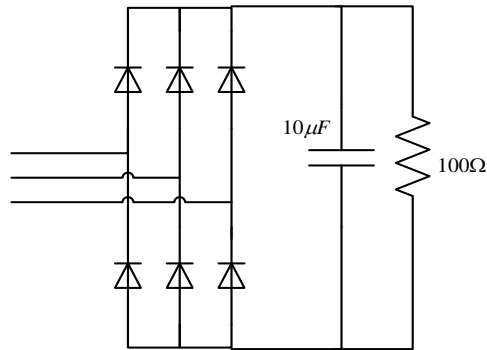
Figure 5-6: Structure of the nonlinear load

5.4   Experimental Tests

The whole setup for the proposed control strategy was implemented experimentally in a real-time simulations hardware in loop (RTHIL) as shown in Fig. 5-7. The plant was simulated in real time using real time digital simulator (RTDS) and the control strategy was developed on dSPACE DS1103 digital controller board prototype as described in [82].
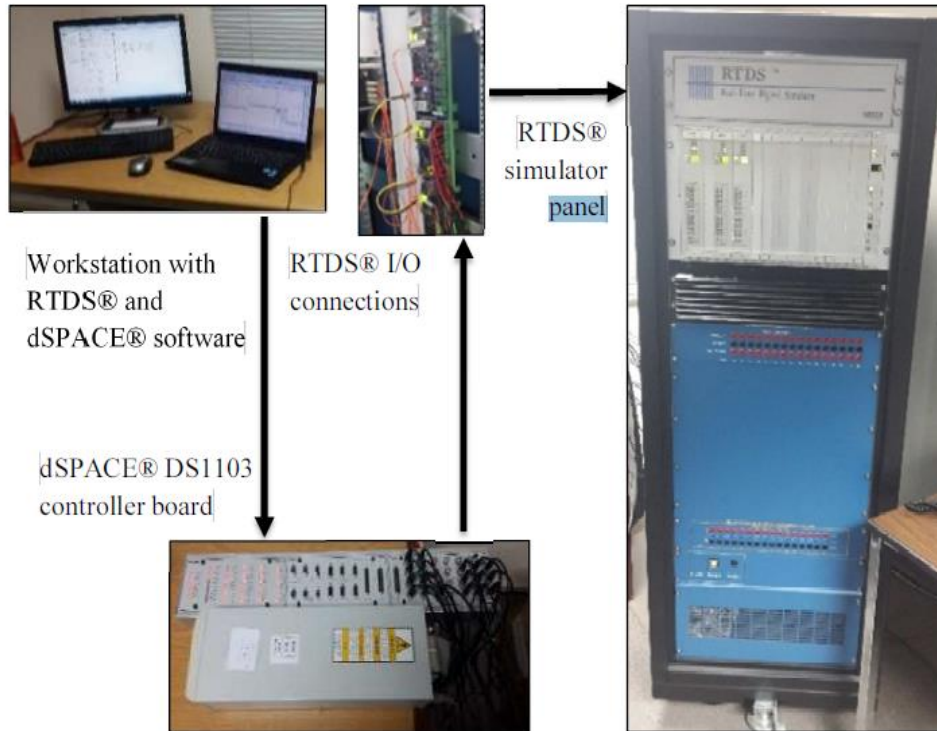
Figure 5-7: Experimental set-up for grid-connected and standalone cases

The workstation houses the RSCAD where the power system is modelled and monitored when compiled and downloaded to the RTDS. Also, the control algorithm was implemented with YALMIP optimization package [83] with MATLAB/SIMULINK and the code generated is deployed to the dSPACE controller interfaced to the RTDS via digital and analog channels. A detailed description of the RSCAD schematics and the controller board is given in the Appendix.

5.4.1 Tracking Results Experimental

The first test carried out to ascertain the effectiveness of this control strategy is the tracking test. This is to ensure how the controller responds to variation in the output voltage within the shortest possible time with the load assumed inductive. The results in Fig. 5-8 show the tracking performance of the controller during transient as well as at 0.45s and 0.6s interval
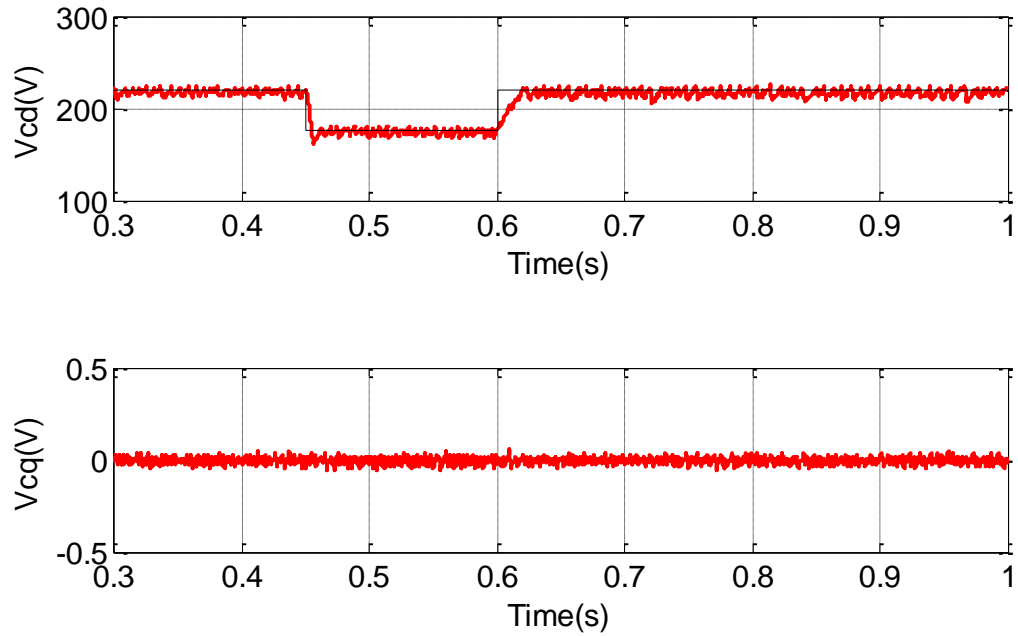
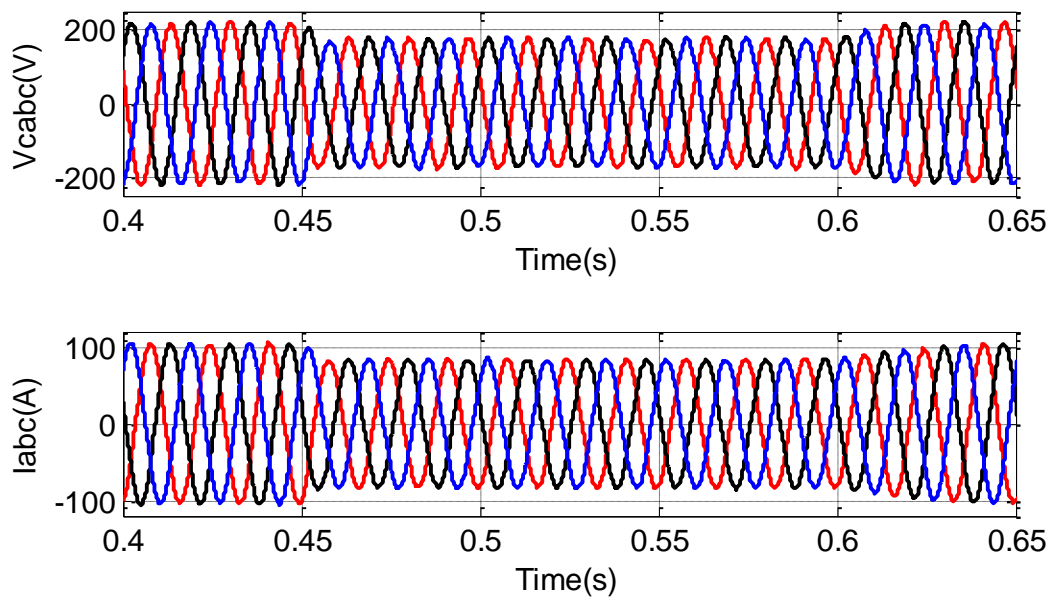Figure 5-8: Output voltage tracking test in d-q frame

Figure 5-9: Output voltage tracking test and load current waveform

during the steady state response when there was 9% dip in the voltage output. In addition,

it can be observed that the coupling between the d-q components of the output voltage $v_c(t)$

is significantly reduced. Fig. 5-8 shows the tracking performance of the output voltage as well as the current drawn from the system in three-phase similar to the simulation case.

5.4.2 Disturbance Test

At steady state, a load disturbance test was carried out. This is to verify that the controller would satisfactorily maintain the output voltage irrespective of the maximum allowable current drawn from the VSI system. This was reflected by changing the nominal resistance of the load by 50% decrease at 0.6s. From Fig. 5-11, more current was drawn from the system and the controller still maintains the output voltage within the prescribed limit. This is reflected in Fig. 5-10 by a short transient dip in $v_{cd}(t)$ and the controller reacted accordingly by maintaining the setpoint before the disturbance. A vivid picture of the change in load current and the controller robustness is well depicted in Fig. 5-11.
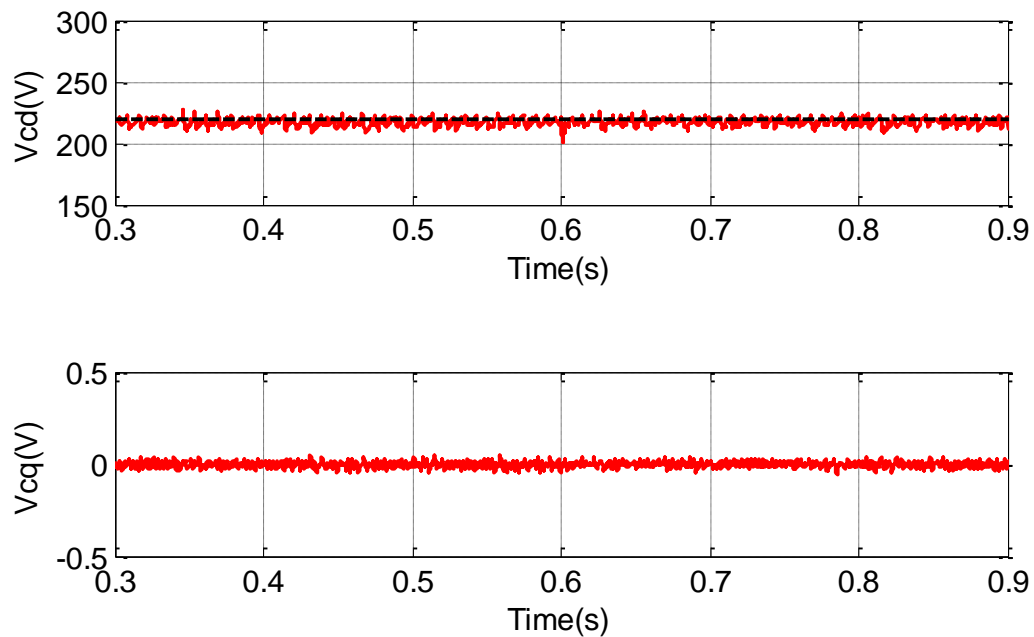

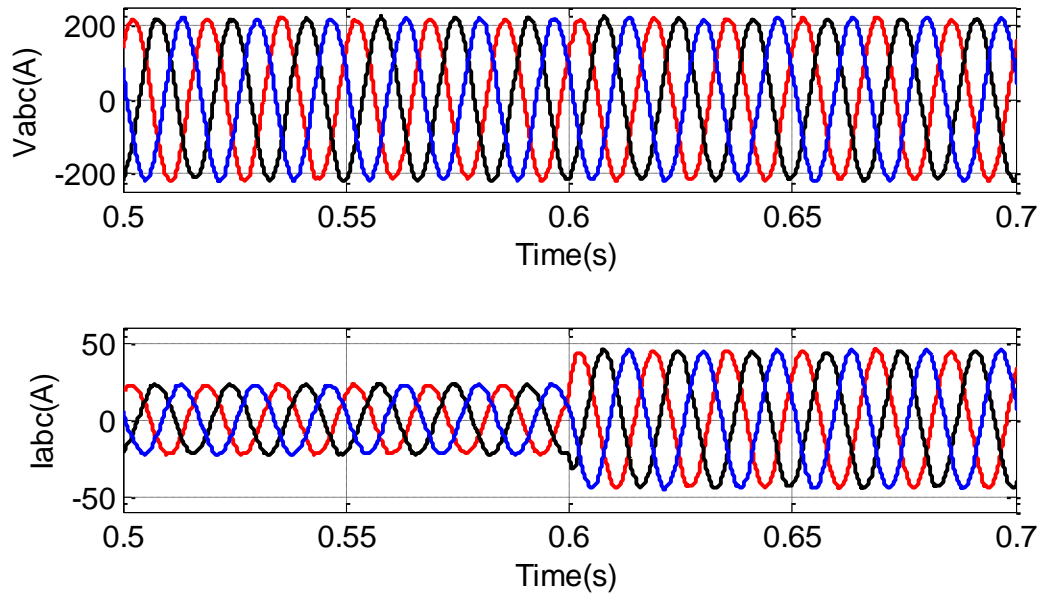**Figure 5-10: Output voltage disturbance test in d-q frame**

Figure 5-11: Output voltage disturbance test and load current

5.4.3 Response to Nonlinear Load

Aside the disturbance test, the controller response to nonlinear load was also tested as demonstrated in the simulation test. The nonlinear load is made of a diode rectifier with RC shunt branch at the output as shown in Fig. 5-5. In Fig. 5-12, the current drawn by the load is highly nonlinear, however, the controller responded well by still regulating the output voltage within the range of the setpoint.

5.4.4 Comparison Test

For a closer look into the validation test, the experimental cases and the simulation cases are superimposed on a single graph in Fig. 5-13. For tracking performance. It can be observed that the two cases follow the required tracking trajectory path. The slight observable difference is in the transient case when there was a change in voltage setpoint.

54

The simulation has a smoother transition period and faster settling time. This is expected to be so due to the hardware and sampling time constraints in the experimental setup.
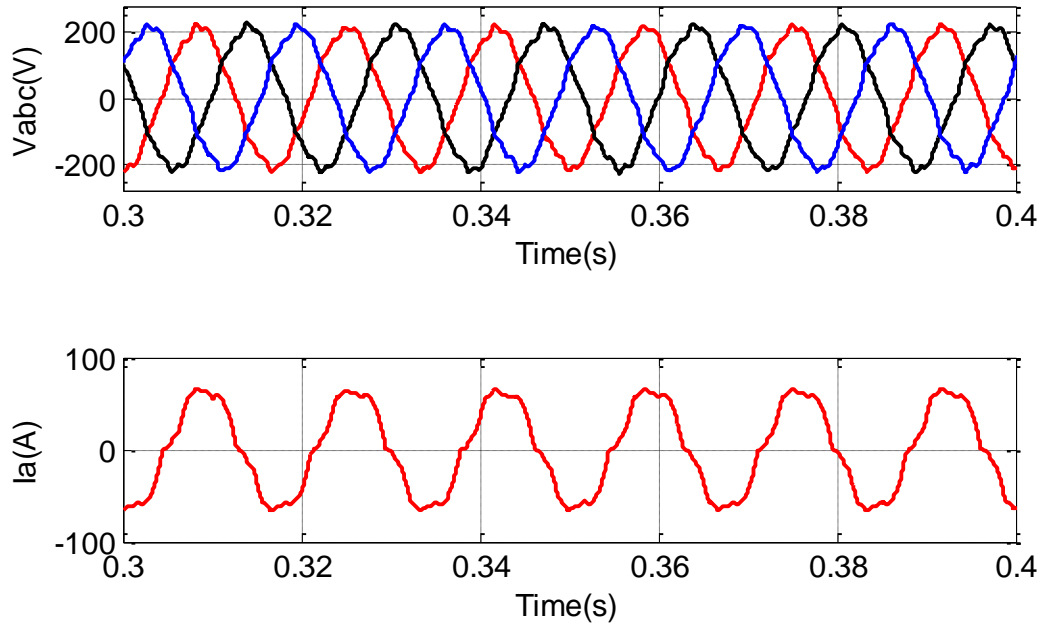

Figure 5-12: Response to nonlinear load current

The proposed control strategy was also compared with an optimal Linear Quadratic Regulator designed separately like the system in [84] but implemented using LMI approach for LQR developed in [85]. It can be observed that the proposed control strategy has a better transient response and decoupling of the d-q output voltage components. The results are shown in Fig. 5-14 and 5-15 for the same system under the same loading condition for comparison purposes.
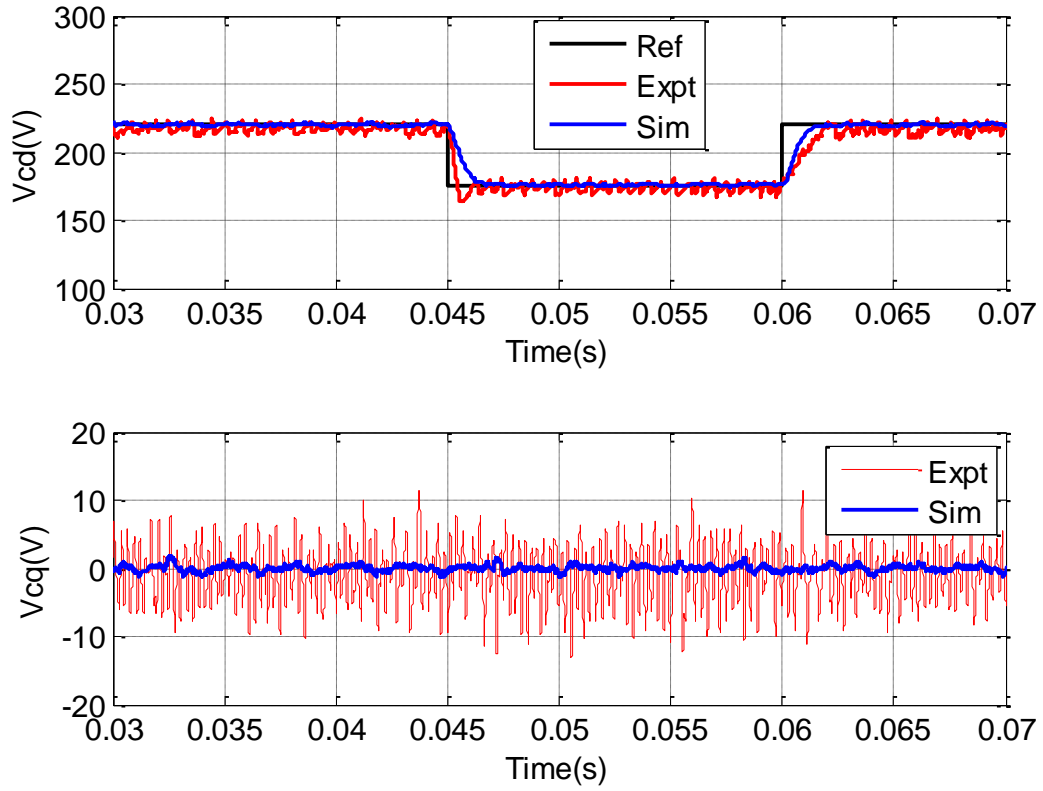
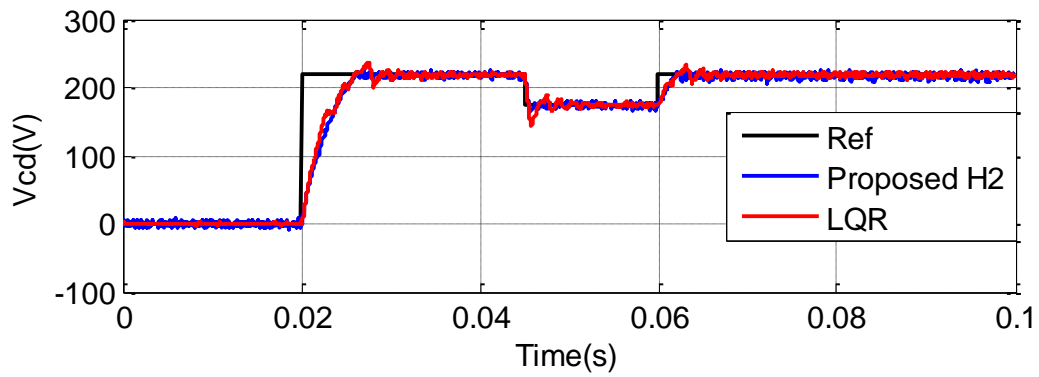**Figure 5-13: Experimental and simulation comparison test**

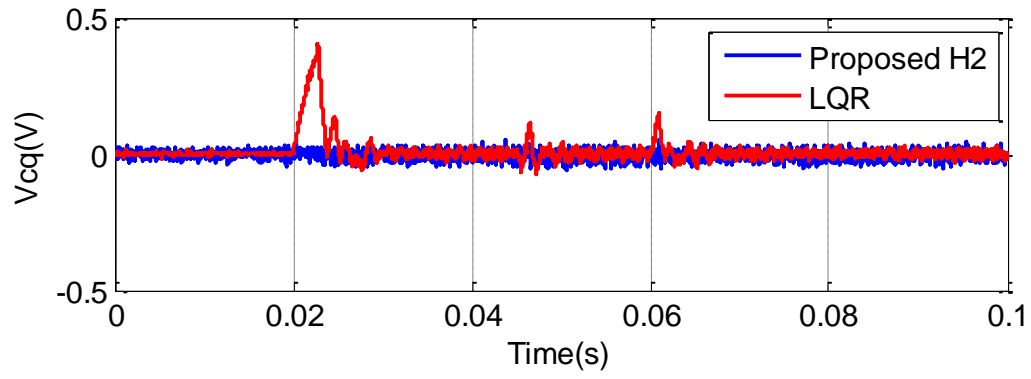Figure 5-14: Comparison with an optimal LQR for dynamic performance

56

Figure 5-15: Comparison with an optimal LQR

CHAPTER 6

RESULTS: GRID-CONNECTED VSI

In this chapter, the results of the simulations and experiments carried out on VSI that can be employed for both microgrid grid-connected mode of operation are presented. The cases studies span tracking test, robustness test and nonlinear load disturbance test.
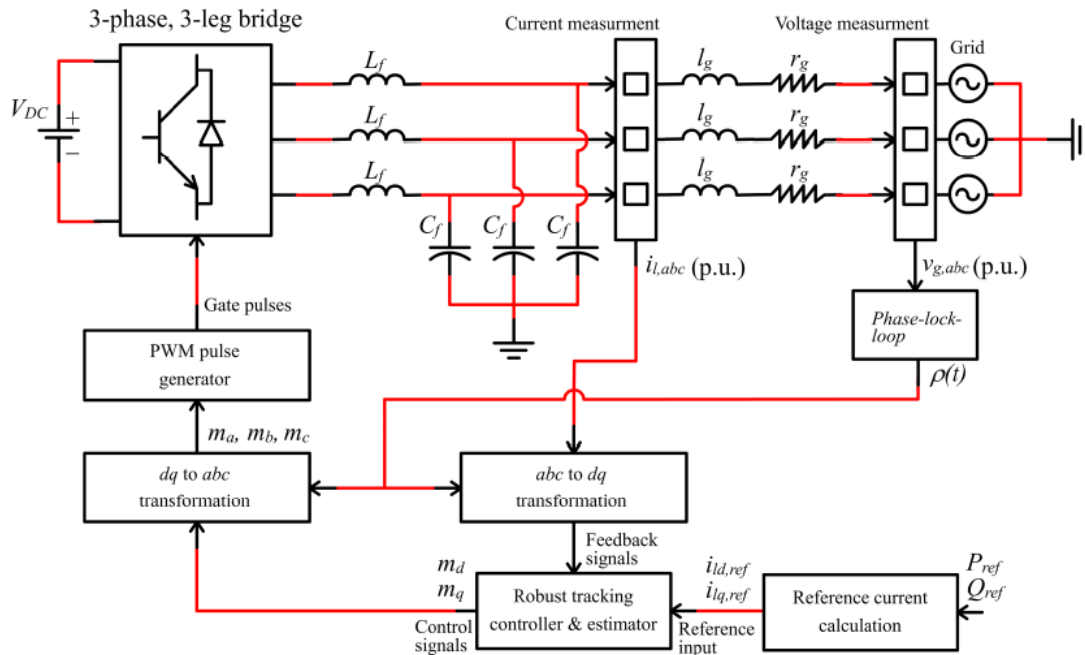
6.1   System Schematics

Figure 6-1: Schematics of the grid-connected VSI [80]

Fig. 6-1 shows a typical single microsource unit with a voltage source inverter interface in a microgrid. As stated in Chapter 5, power sources are represented by a constant voltage source with the assumption that the DC link capacitor voltage is well regulated. Therefore, the controller is not shown. Also, the 2-level inverter is fed with pulses from the PWM triggered by the robust optimal controller.

The controller is implemented in the d-q reference frame, therefore, there is a necessity for signal transformation block from a-b-c frame to d-q frame and vice versa. The transformation units are synchronized with the system using a PLL. Because the output voltages from the inverter have large harmonic contents, it is customary to append L, LC, or LCL filter for harmonic suppression. In this work, an LC filter is used. It is preferable to L filter especially in terms of cost and size. However, for LC and LCL filters, there is usually a problem of resonance. Hence, the control design becomes more complex.

The VSI unit with the filter structure are also interfaced to the low voltage bus via coupling inductance which could be modelled as parasitic resistance and an inductance in series as shown in Fig 6-1. It is also possible that the microgrid could feed local loads. Therefore, loads are connected to the low voltage bus via breakers. An overall picture of the single-phase representation of the system with its control is shown in Fig 6-2.
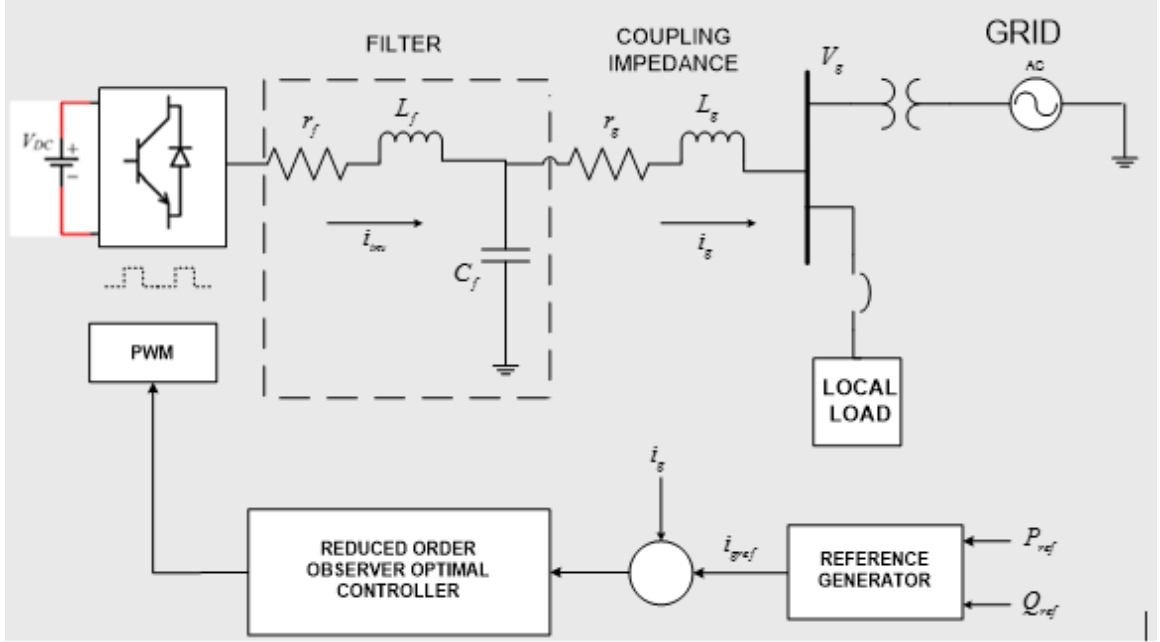
Figure 6-2: Single-phase model of the grid-connected VSI

6.2 System and Controller Parameters

The choice of system parameters for the simulation and experimental work are not arbitrary. Rather, they were chosen according to the parameters used in [86] which are shown in Table 6-1. The controller parameters after results of the convex optimization of (4.41) to (4.43) and observer gain from MATLAB using pole placement technique are shown in Table 6-2. Also, the at the steady state of the PLL, the reference value for the grid current is calculated from the reference active and reactive powers as follows

$$\begin{bmatrix} i_{dref}(t) \\ i_{qref}(t) \end{bmatrix} = \frac{1}{V_{gd}(t)} \begin{bmatrix} \frac{2}{3} P_{ref} \\ \frac{-2}{3} Q_{ref} \end{bmatrix} \tag{6.1}$$

where $i_{dref}(t)$ and $i_{qref}(t)$ are the reference current to the controller in d-q frame. Also, the grid q-component $V_{gq}(t)$ is zero at the steady state of the PLL.

Table 3: System Parameters

Parameter	Symbol	Value
DC Voltage	V_{dc}	480V
Frequency	f	60Hz
Phase value low voltage grid	V_g	220V
Filter Inductance	L_f	0.8mH
Filter Line Resistance	r_f	0.1Ω
Filter Capacitance	C_f	75μF
Nominal Line Resistance	r_g	0.4Ω
Nominal Line Inductance	l_g	1μH
Grid resistance variation	Δr_g	[0.4 0.5]Ω
Grid Inductance variation	Δl_g	[1 100]μH
Sampling Time	T_s	2.5μs
Controller Sampling Time	T_{samp}	10μs

Table 4: Controller Parameters

Parameter	Value
γ	0.25
K_{opt}	$\begin{bmatrix} 239.20 & 0.13 & 81.92 & 0.57 & -13.41 & 0.13 & -8.9e4 & 871.39 \\ -0.18 & 239.20 & -0.61 & 81.92 & -0.12 & -13.41 & -844.18 & -8.9e4 \end{bmatrix}$
L	$\begin{bmatrix} -5.96 & -0.075 & -0.71 & -0.0056 & -1.35 & -0.008 \\ -0.11 & -5.77 & -0.0089 & -0.7 & -0.014 & -1.33 \end{bmatrix}^T$

6.3   Simulation Results

To verify the effectiveness of the proposed controller, simulation tests for three different cases were carried out in MATLAB/SIMULINK as depicted in the schematic in Fig. 6-1. The system parameters used for the simulation cases are given in Table 6-1. Also, the controller gain parameters for the observer-based controller are also shown in Table 6-2. These parameters are also used for the experimental cases. Also, the whole SIMULINK blocks used for the simulations are shown in Appendix B.

6.3.1   Tracking Results Simulation

In this test, tracking performance test was carried to verify how the controller responds to change in active and reactive power demand. It can be observed in Fig. 6-3 and Fig. 6-4 that controller gave a pretty good transient response without overshoot and tracks the changes in the active and reactive power sufficiently. Another interesting observation is that the coupling between the active and reactive power is significantly reduced. Hence, aside the good tracking performance, the controller has capability to decouple all couple terms in the system. Also Fig. 6-5 also shows the tracking performance of the grid currents in d-q frame and three-phase respectively.
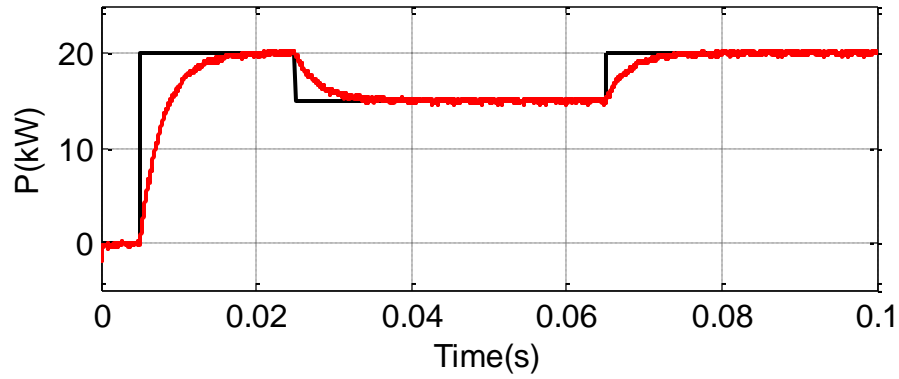
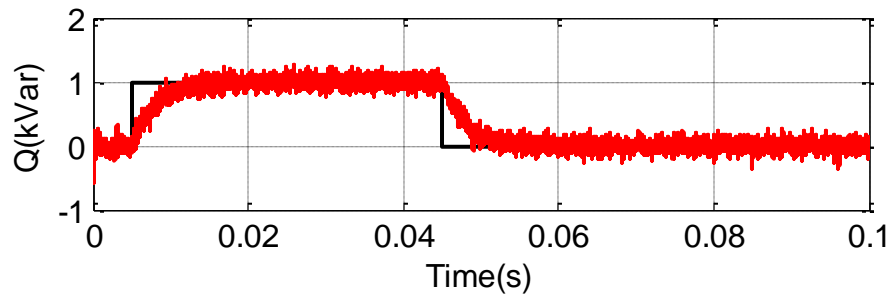**Figure 6-3: Active demand power tracking test**

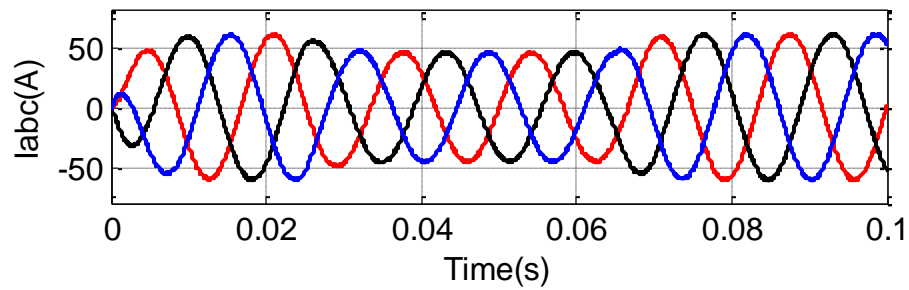**Figure 6-4: Reactive power demand tracking test**

Figure 6-5: Grid current in d-q frame three-phase

6.3.2 Resistive Load Response Test

In this test, the resilience of the controller is put to test. Initially, when the system reaches

steady state, there was no local load connected to the microgrid. In Fig. 6-6, At 0.04s, a

resistive load of 12Ω is connected to the system at the microgrid low voltage bus. This

disrupts the active power demand and reactive power set-point within a very short period of time and the system recovers back to the previous steady state. The disturbance caused by the connected load is shown in the grid current waveform displayed in Fig. 6-7
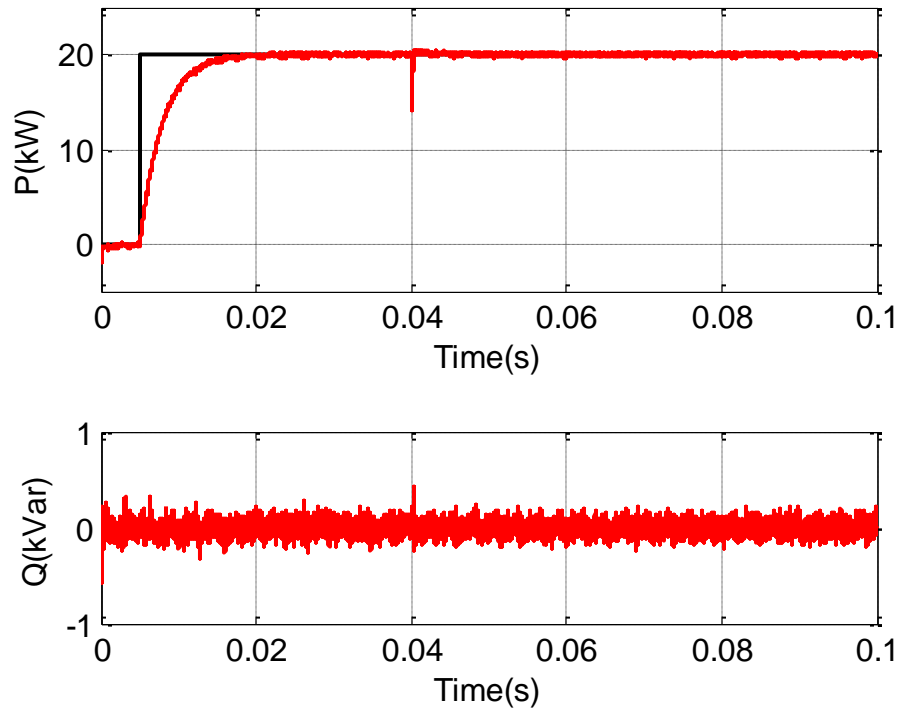

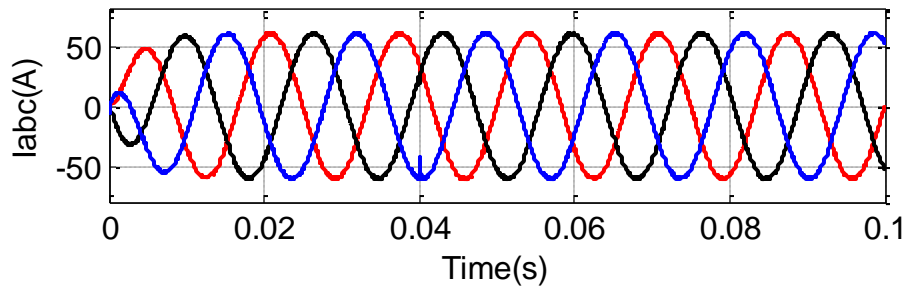**Figure 6-6: Active and reactive power upon load connection to the system**

Figure 6-7: Grid-current during load connection

6.3.3 Simulation with Nonlinear Load

Aside the connection of resistive load to the system, a nonlinear load, as in the case in Chapter 5 is connected to the system at 0.04s. From Fig 6-8, we could see that nonlinearity of the load impacted the active and reactive power profile and the power by making it less distorted. Despite, the distorted load current drawn from the system, as in Fig. 6-9, the grid current still maintains the desired response. However, the overall THD is increased but it is still within the acceptable limit and the system remains stable. This is illustrated in Fig. 6-10
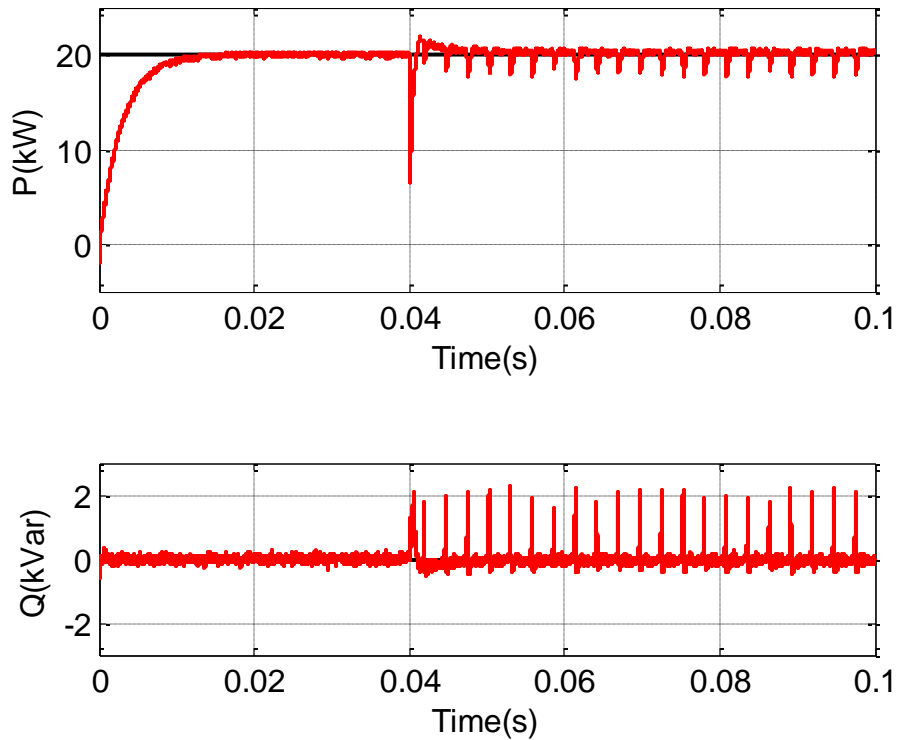

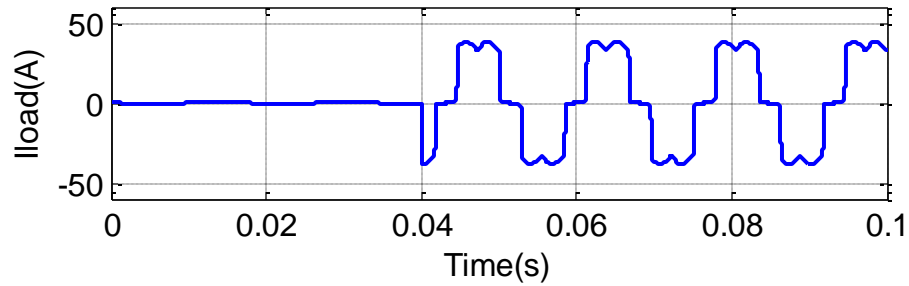**Figure 6-8: Active and reactive power due to nonlinear load connection**

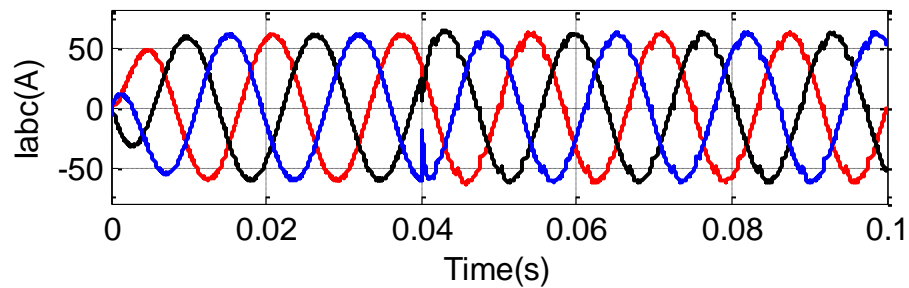**Figure 6-9: Nonlinear load current profile**

Figure 6-10: Response to nonlinear load connection

6.4 Experimental Tests

The whole setup for the proposed control strategy was implemented experimentally in a real-time simulations hardware in loop (RTHIL) as shown in Fig. 5-7. The plant was simulated in real time using real time digital simulator (RTDS) and the control strategy was developed on dSPACE DS1103 digital controller board prototype as described in [82]. Also, the control algorithm was implemented with YALMIP optimization package [83] with MATLAB/SIMULINK and the code generated is deployed to the dSPACE controller interfaced to the RTDS via digital and analog channels. The parameters for the experimental work are given in the Table 6-1.

6.4.1 Tracking Results Experimental

The first test carried out to ascertain the effectiveness of this control strategy is the tracking test. This is to ensure how the controller responds to variation in the output voltage within the shortest possible time in real time using a real controller prototype. The result in Fig. 6-11 show the tracking performance of the controller during transient as well as at 0.025s and 0.065s interval during the steady state response when there was 20% dip in the active power demand and output. Also, changes in the reactive power demand was adequately tracked as seen in Fig 6-12. In addition, it can be observed that the couplings between the d-q components of the powers and the currents are significantly reduced as it can also be seen in Fig. 6-11 and Fig. 6-12. Fig. 6-13 shows the tracking performance of the current fed to the grid in three- phase.
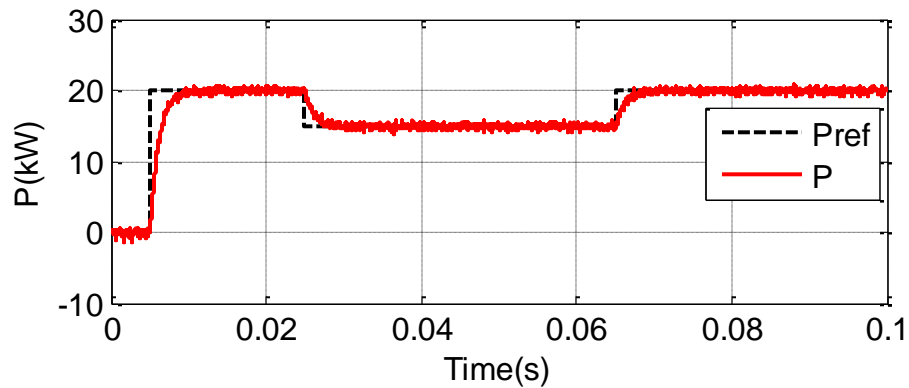

Figure 6-11: Tracking active power demand
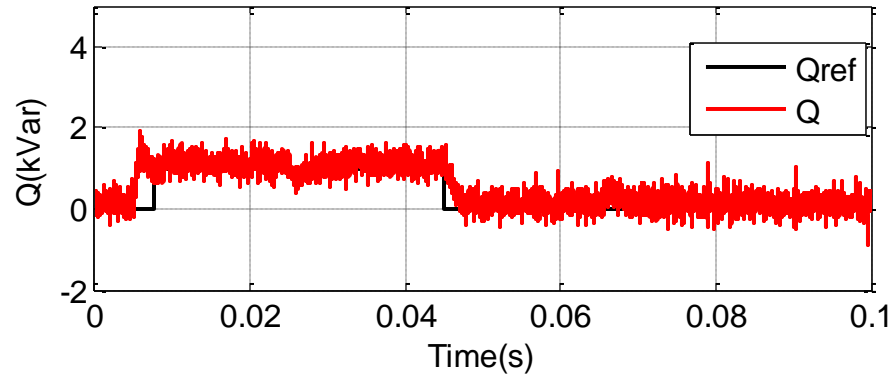
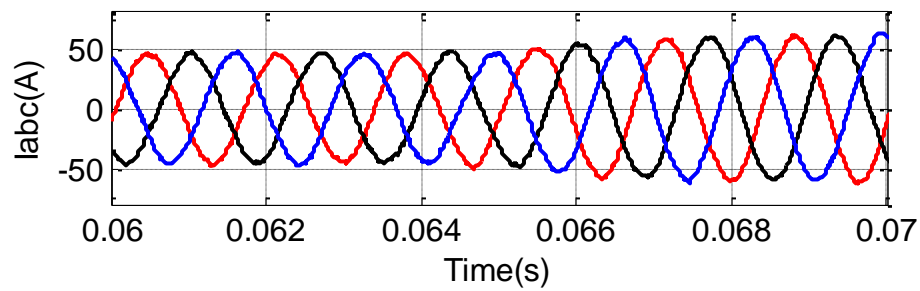**Figure 6-12: Tracking reactive power demand**

Figure 6-13: Grid current in three-phase during tracking

6.4.2 Disturbance Test

At 0.05s, an inductive load with parameters like the case in Table 6-1 was connected to the system. There was a dip in active power due to the sudden addition of load for a very short
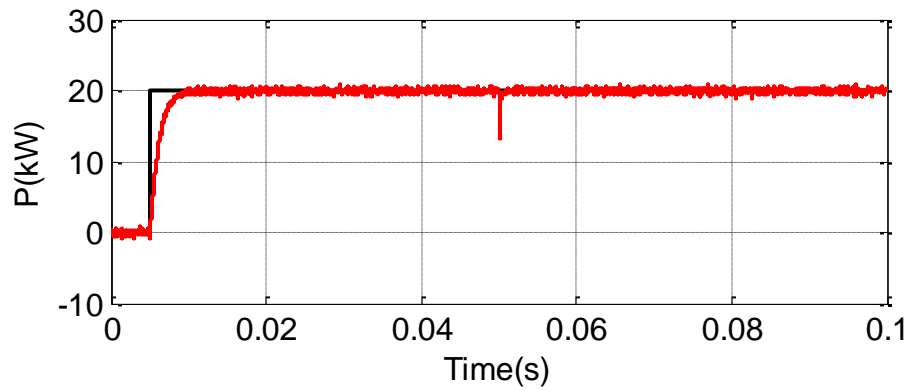

Figure 6-14: Active power response for disturbance test

period as it is shown in Fig. 6-14. Also, the load addition is reflected as a surge in the reactive power set-point as depicted in Fig. 6-15.
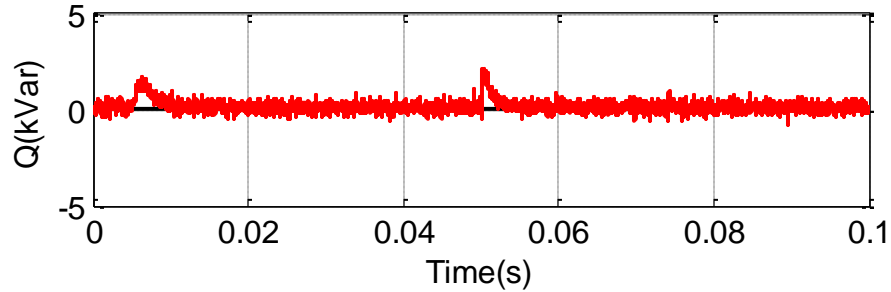
Figure 6-15: Reactive power response to load disturbance
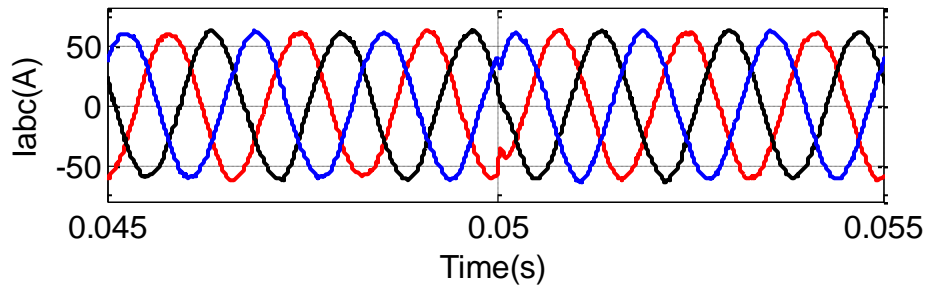
Figure 6-16: Grid current response to load disturbance test

6.4.3   Response to Nonlinear Load

Like the load disturbance test, a nonlinear load shown in Fig. 5-6 is connected to the microgrid at the low voltage bus to ascertain the response of the system to such loads with high nonlinearity. The nonlinear load was switched on to the system at 0.05s. The controller quickly responds to the load addition and recovers back to the steady state as shown in active and reactive power demand response in Fig. 6-17 and Fig. 6-18 respectively. However, there is a slight increase in the THD as the system continues to supply the nonlinear load. This is because the nonlinear load draws nonlinear current which also impacts the quality current being fed to the grid. The system response is shown in Fig 6-19.
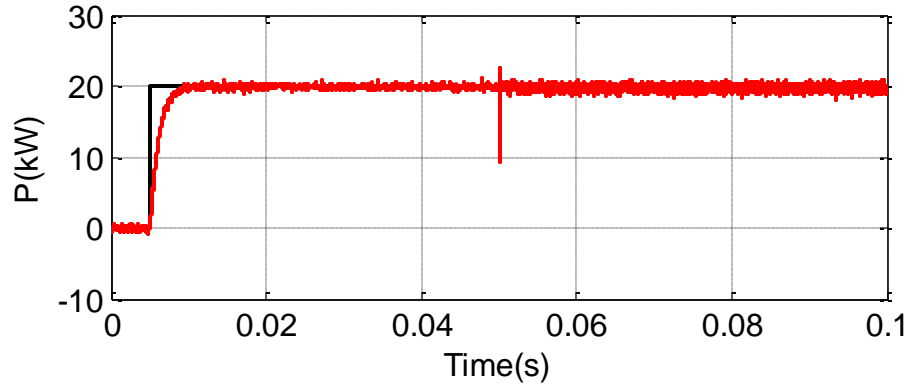
Figure 6-17: Active power response to nonlinear load addition
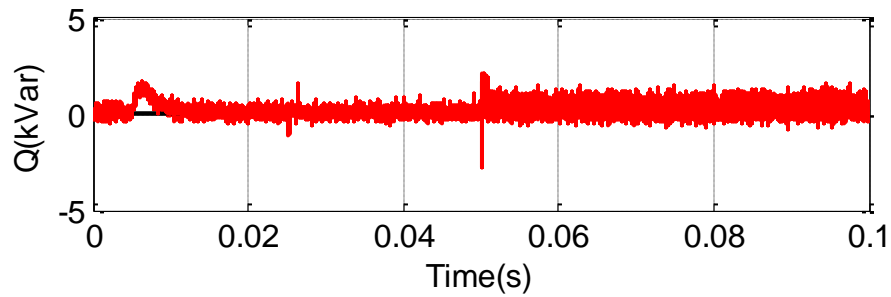
Figure 6-18: Reactive power response to nonlinear load addition
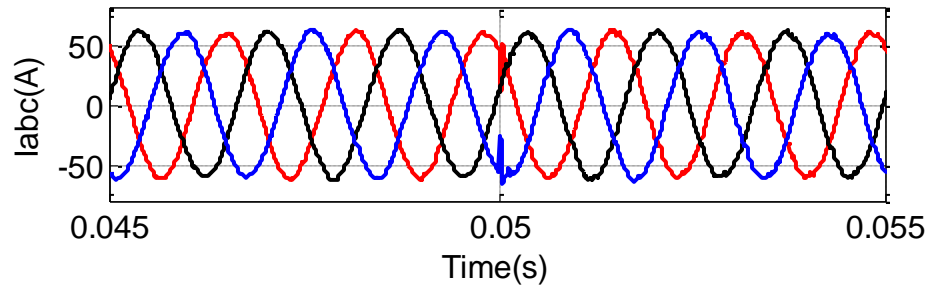
Figure 6-19: Response to nonlinear load addition to the microgrid

6.4.4 Qualitative Analysis

As mentioned in the objective of this proposed active damping current control strategy, it is necessary that THD of the current being injected into the grid is less than 5% as dictated by the IEEE 1547 standard. In that case, the data for the experimental of different case studies were collected and analyzed in MATLAB/SIMULINK using Fast Fourier

70

transform (FFT) approach to calculate the THD of each phase of the current fed to the grid. So, the THD of four different cases in the steady state are tabulated in Table 5. For the case of maximum allowable grid inductance and resistance, the quality degrades less when compared with the no load case with nominal inductance value. As for when the loads are switched on to the system, the THD increased a bit in the two cases but still within the THD limit allowable.

<div align="center">

Table 5: THD of different case studies

Load Type	THD (%)		
	Phase a	**Phase b**	**Phase c**
No load	2.17	2.64	2.49
No load with maximum value of L_g	2.75	2.61	2.63
Resistive load	3.27	3.32	2.98
Nonlinear Load	3.36	3.50	3.61

</div>

6.4.5 Comparison Test

In this case, the controller designed in this work is compared with the results of another robust controller designed for the same system using the same system parameters. Also, the same experimental set-up was used to carry out all the case studies. Hence, the comparison is fair. For the comparison, the tracking test is only considered. As it can be seen in Fig 6-20, the transient phase of the proposed controller in Fig 6-11 is better. Unlike in Fig 6-20 where there is an appreciable overshoot, the active power profile of the proposed controller glides to the steady states without overshoot during the same transient
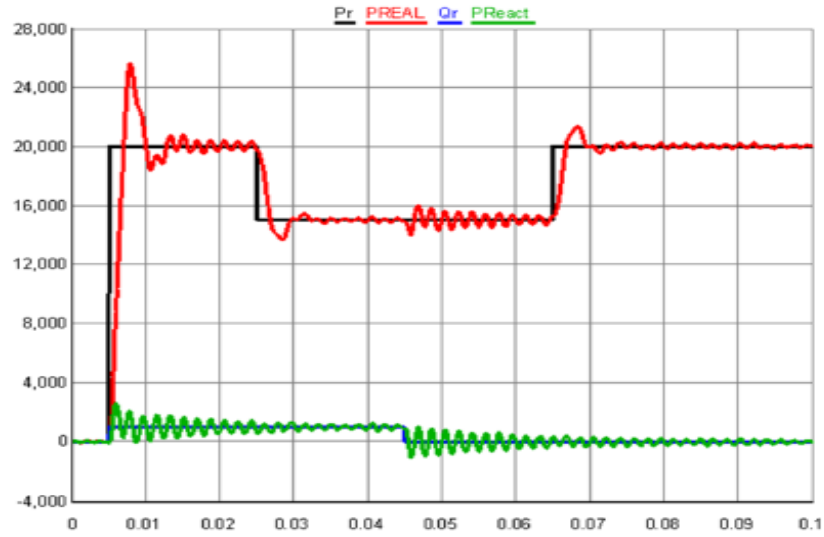
Figure 6-20: Active and reactive power tracking test from [80]

period. Another distinguishing feature of the results proposed controller in Fig 6-11 and

Fig 6-12 when compared with that in Fig 6-20 is the inherent decoupling of the d-q channel.

In other words, the changes in the active power demand has insignificant effect on the

reactive power demand vice versa. Whereas, in Fig 6-20, there is a noticeable coupling

between the active and reactive power demand.

CHAPTER 7

CONCLUSION AND FUTURE WORK

Wide range of control strategies have been employed to enable the successful integration of DER to grid via microgrid solution. In this work, an optimal robust controller based on H_2 norm minimization has been proposed to achieve control of VSI used in microgrids in standalone and grid-connected mode. Also, this proposed control strategy is also well-suited for UPS applications.

7.1   Conclusion

In this work, a robust optimal control strategy was proposed for a VSI employed in microgrid during standalone and grid-connected mode. For the standalone case, the objective of the control strategy was to regulate the microgrid voltage irrespective of the events around the system. Therefore, the controller was designed to ensure sufficient regulation of the microgrid voltage irrespective of the type of loads connected at its terminal. The control law is the result of a convex optimization of a set of LMI. This was originally formulated as minimizing the effect of the disturbance on the output while ensuring the system remains stable. The effectiveness of the proposed controller was put to test by simulation and experimental cases. For all the tests considered in both cases, the controller had good performances in terms of tracking, robustness, and disturbance rejection.

In the grid-connected mode, the voltage and frequency of the microgrid supported by the grid. Therefore, the objective of the control strategy was to ensure the microgrid supplies

less distorted sinusoidal currents to the grid. Therefore, the controller was designed in such a way to ensure the VSI system supplies less distorted current reflected as power demand irrespective of the type of loads connected at the AC bus and the changes in the coupling inductance within the allowable variation. The control law is the result of a convex optimization of a set of LMI. This was originally formulated as minimizing the effect of the disturbance on the output while ensuring the system remains stable. The effectiveness of the proposed controller was put to test by simulation and experimental cases. For all the tests considered in both cases, the controller had good performances in terms of tracking, robustness, and ruggedness.

7.2   Future Work

The following points are worthy of recommendation to improve on this work:

- Since the proposed controller has only been adopted for grid feeding and forming VSI, it is recommended for future work to employ this control strategy for VSI operating in the grid supporting case which can subsequently be used for parallel operation of many VSI.
- Also, value of the filter inductance and capacitance should be given a more careful design consideration based on the size of the system.
- In this work, the controller and observer gains were designed independently. To have an exclusive robust controller, it is required to incorporate the observer design into the control problem formulation.
- Although, in the optimization process, there is only one free variable that determines the closed loop performance of the system. This was tuned manually.

For specific design specifications, heuristic techniques could be used to achieve the optimum value of the variable that meets the design goals.

- A multi-objective approach to the controller design is feasible. Especially for the grid connected case, the control objective could be to ensure quality current being fed to the grid while minimizing the effect of the current drawn by the load as well as the event at the grid side.

- For the experimental case, RTHIL was used. Instead, a more practical set-up could be adopted by using real inverters with the controller board used in this work.

APPENDIX

SIMULINK AND RTDS SCHEMATICS

1. Simulink Diagram
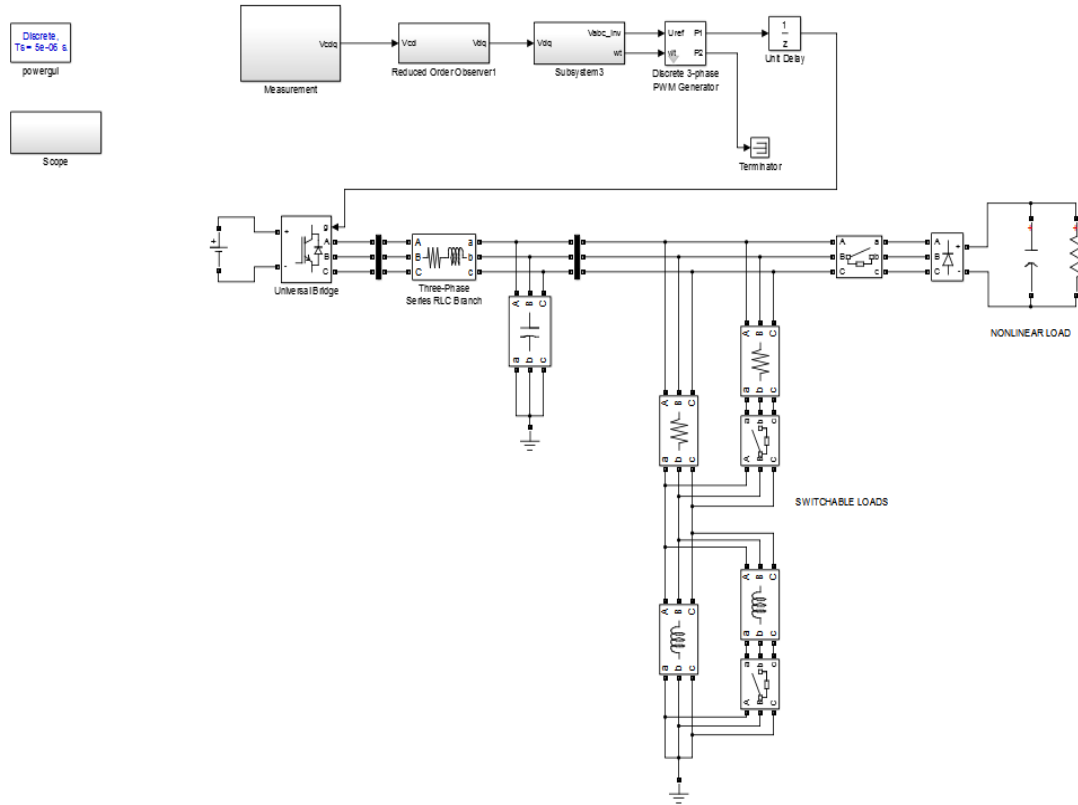
Figure A-0-1: Power system model of the VSI in standalone mode

Fig. A-1 and Fig A-2 shows the Simulink file implemented for the VSI in the standalone and grid-connected mode respectively. The input to the inverter is assumed to be a well-regulated constant direct current (DC) voltage source. Also, rest of the system are easily identified as shown in the figures. Fig. A-3 shows the measurement block needed for the output feedback in the standalone mode. This is also similar for the grid-connected case.

Fig. A-4 shows the graphical implementation of the observer based controller with Fig. A-

5 showing how the controller parameters were entered.

Figure A-0-2: Power system model of the VSI in grid-connected mode

Figure A-0-3: Output signal measurement
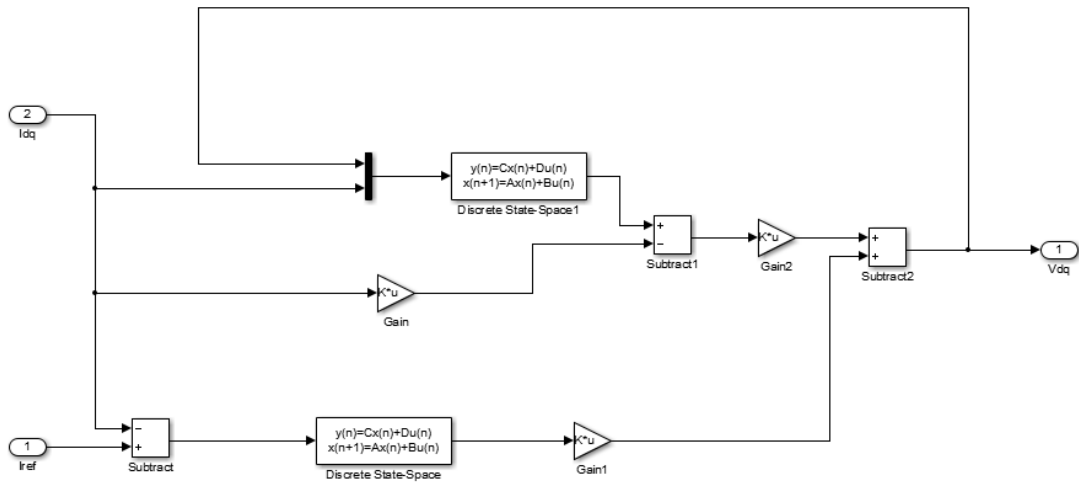
Figure A-0-4: Reduced order observer controller block
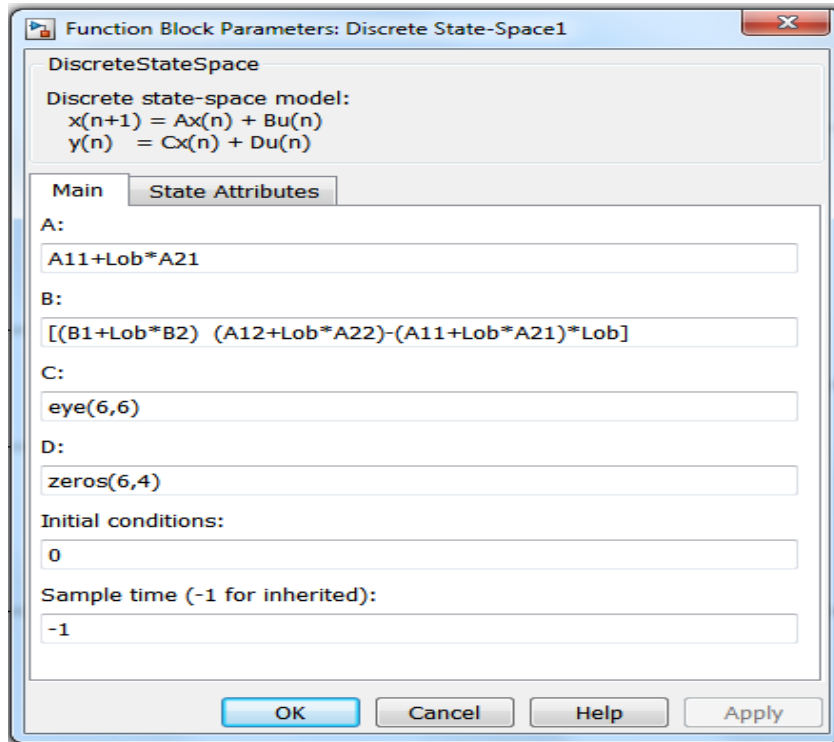
Figure A-0-5: State space parameter values from MATLAB workspace

78

2. RSCAD schematics in RTDS

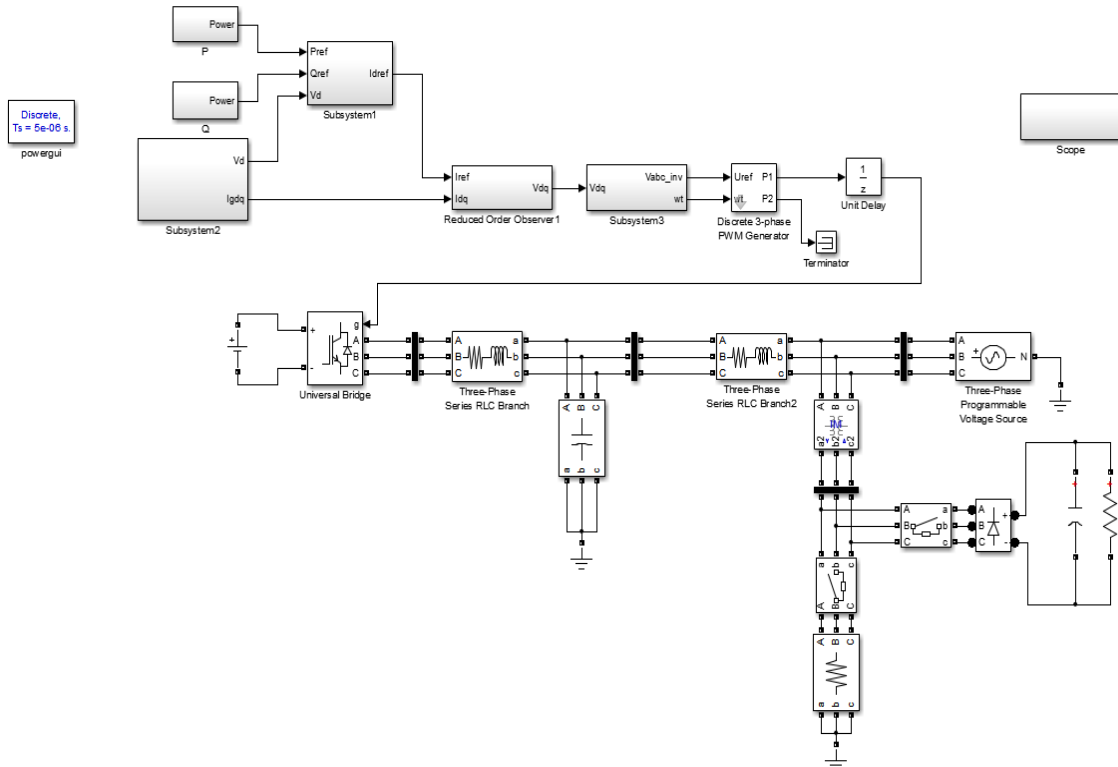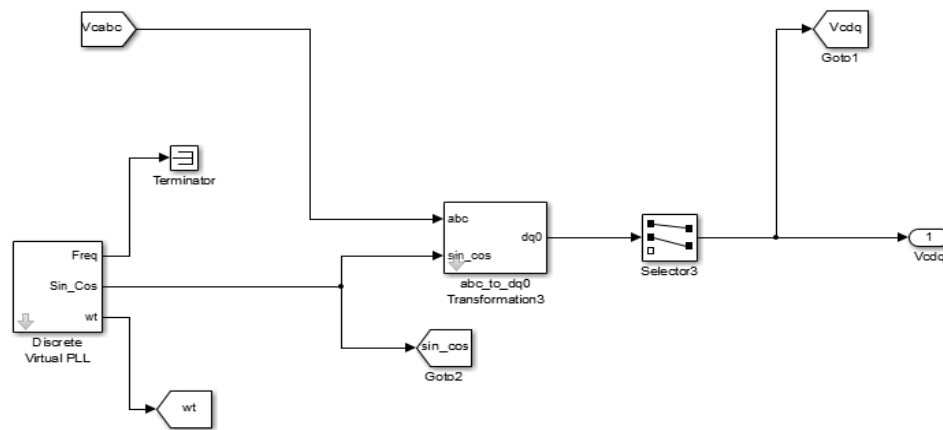In the RSCAD, the draft files needed for the RTDS simulation are discussed below. Like the Simulink file, the standalone mode is drafted as shown in Fig. A-6 in small time-step module. Also, another draft is implemented for the grid-connected mode in Fig. A-7 with little modification of Fig. A-6 by including the grid source voltage and coupling inductance.

In the large time step environment, the interface and measurement unit are drafted. In Fig. A-7, shows the analog and digital channel necessary for the transfer of control signals from the RTDS to the dSPACE and vice versa. Fig. A-9 shows how a single block is implemented for the controller by entering the state space matrices of the observer-based controller as discussed in Chapter 3. This is done in Simulink and code generated are downloaded to the controller board for implementation.

Finally, Fig. A-10 shows how the measurement units are used to implement necessary system variables needed in RTDS and dSPACE interaction.

Figure A-0-6: Draft file for the VSI in the standalone mode

Figure A-0-7: System circuit for island and grid-connected mode

Figure A-0-8: Input and output interface with the real controller

Figure A-0-9: Controller interface with RTDS

Figure A-0-10: Transformation of three phase signals to d-q frame

REFERENCES

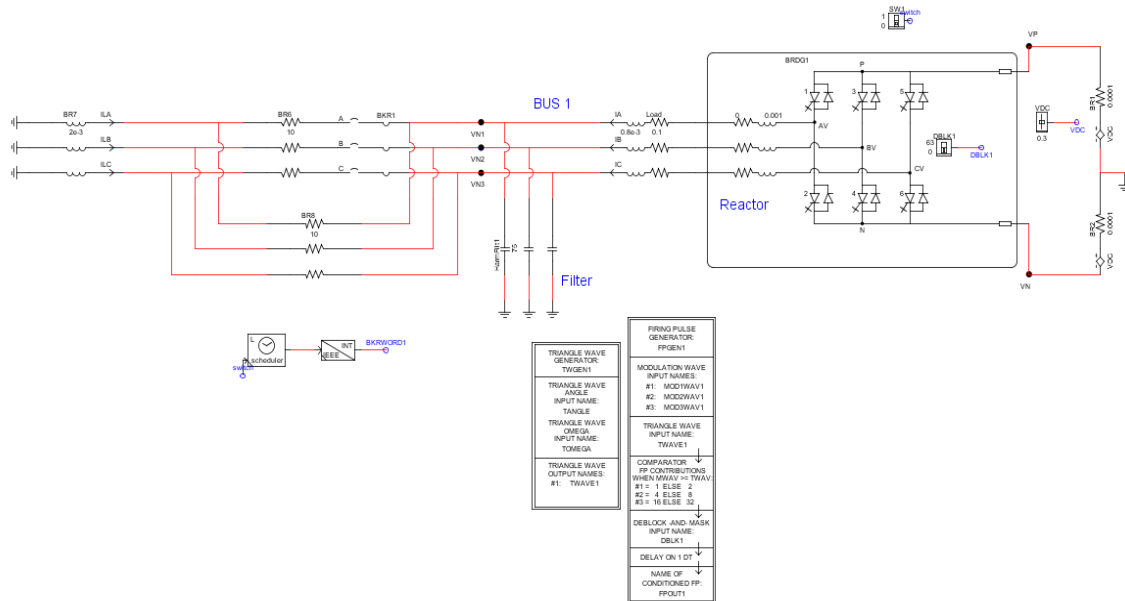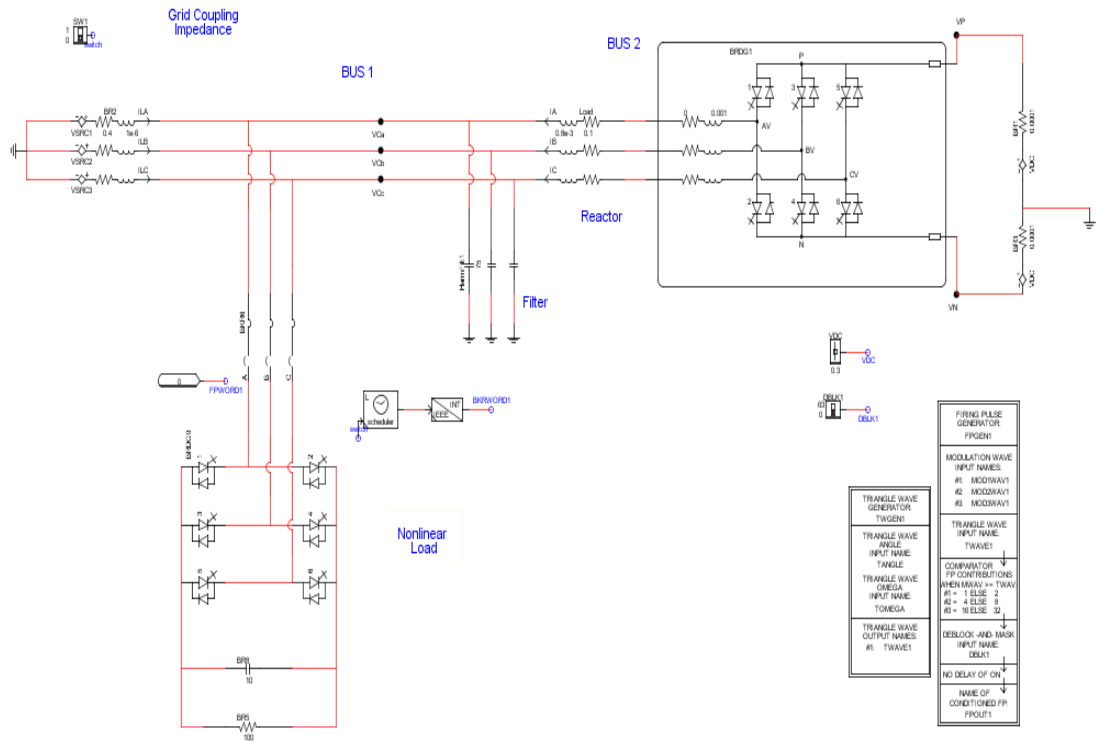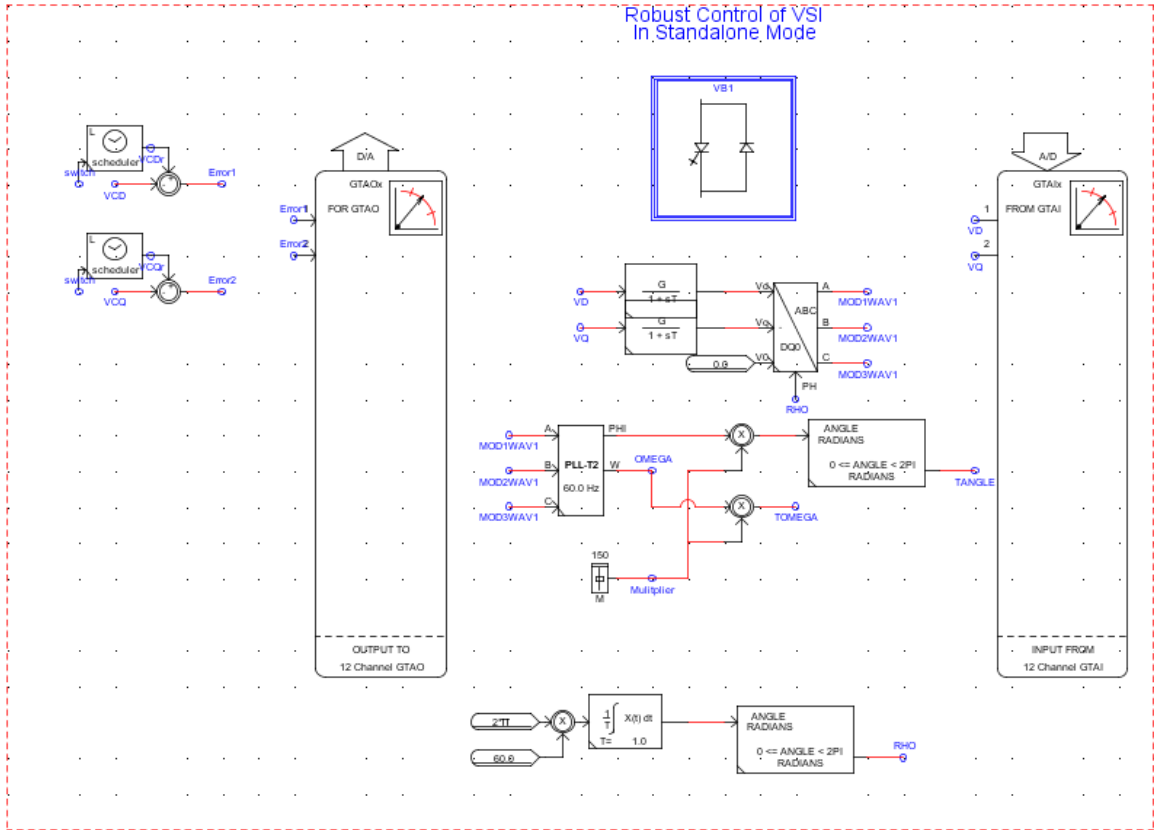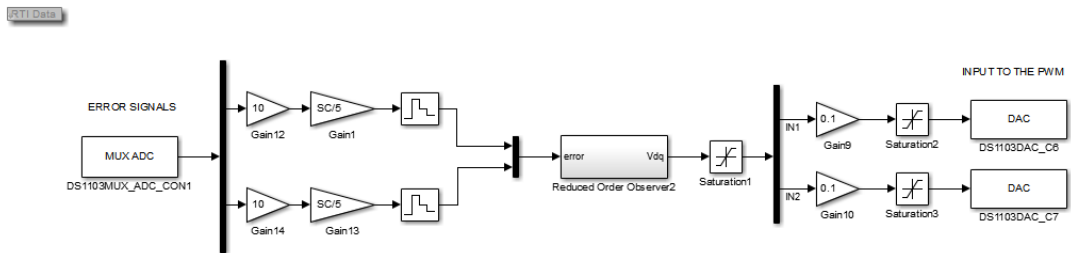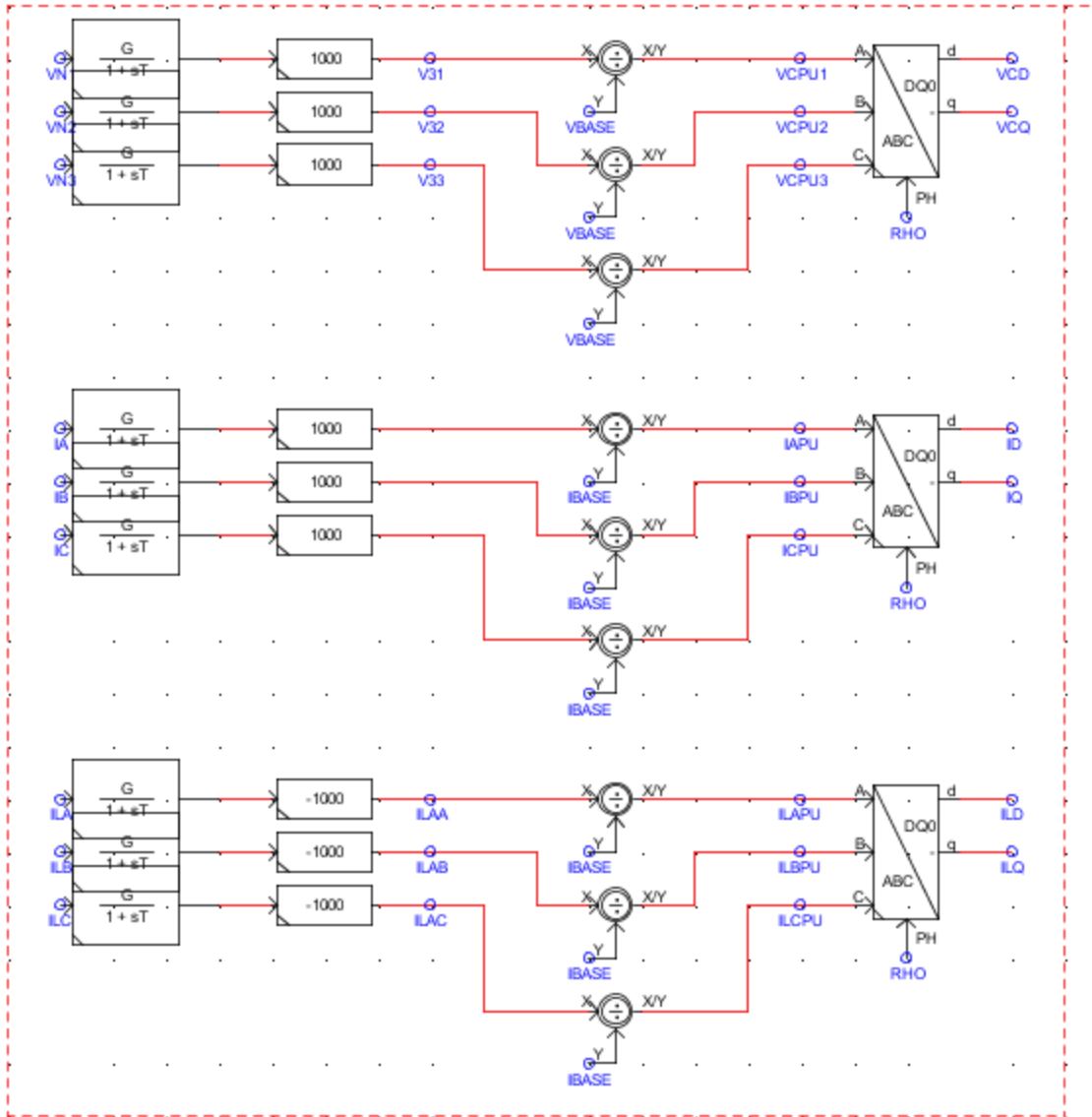[1]   R. H. Lasseter, "MicroGrids," *2002 IEEE Power Engineering Society Winter Meeting. Conference Proceedings (Cat. No.02CH37309)*, vol. 1, pp. 305–308, 2002.

[2]   P. Piagi and R. H. Lasseter, "Autonomous control of microgrids," *2006 IEEE Power Engineering Society General Meeting*, p. 8 pp., 2006.

[3]   J. A. P. Lopes, C. L. Moreira, and A. G. Madureira, "Defining control strategies for microgrids islanded operation," *IEEE Transactions on Power Systems*, vol. 21, no. 2, pp. 916–924, 2006.

[4]   R. H. Lasseter and P. Paigi, "Microgrid: A conceptual solution," *PESC Record - IEEE Annual Power Electronics Specialists Conference*, vol. 6, pp. 4285–4290, 2004.

[5]   B. Kroposki, R. Lasseter, T. Ise, S. Morozumi, S. Papathanassiou, and N. Hatziargyriou, "Making microgrids work," *IEEE Power and Energy Magazine*, vol. 6, no. 3, pp. 40–53, 2008.

[6]   T. C. Green and M. Prodanovi??, "Control of inverter-based micro-grids," *Electric Power Systems Research*, vol. 77, no. 9, pp. 1204–1213, 2007.

[7]   D. E. Olivares *et al.*, "Trends in microgrid control," *IEEE Transactions on Smart Grid*, vol. 5, no. 4, pp. 1905–1919, 2014.

[8]   N. Hatziargyriou, H. Asano, R. Iravani, and C. Marnay, "Microgrids," *IEEE Power and Energy Magazine*, vol. 5, no. 4, pp. 78–94, 2007.

[9]   K. S. Rajesh, S. S. Dash, R. Rajagopal, and R. Sridhar, "A review on control of ac microgrid," *Renewable and Sustainable Energy Reviews*, vol. 71, no. January, pp. 814–819, 2017.

[10]   P. P. Varaiya, F. F. Wu, and J. W. Bialek, "Smart Operation of Smart Grid: Risk-Limiting Dispatch," *Proceedings of the IEEE*, vol. 99, no. 1, pp. 40–57, 2011.

[11]   J. A. P. Lopes, N. Hatziargyriou, J. Mutale, P. Djapic, and N. Jenkins, "Integrating distributed generation into electric power systems: A review of drivers, challenges and opportunities," *Electric Power Systems Research*, vol. 77, no. 9, pp. 1189–1203, 2007.

[12]   N. Pogaku, M. Prodanović, and T. C. Green, "Modeling, analysis and testing of autonomous operation of an inverter-based microgrid," *IEEE Transactions on Power Electronics*, vol. 22, no. 2, pp. 613–625, 2007.

[13]   C. Hou, X. Hu, and D. Hui, "Hierarchical Control Techniques Applied in Mi-cro-grid," in *International Conference on Power System Technology*, 2010, pp. 1–5.

[14] A. Tavakoli, M. Negnevitsky, S. Lyden, and O. Haruni, "A decentralized control strategy for multiple distributed generation in islanded mode," *2014 IEEE PES General Meeting | Conference & Exposition*, pp. 1–5, 2014.

[15] J. M. Guerrero, M. Chandorkar, T.-L. Lee, and P. C. Loh, "Advanced Control Architectures for Intelligent Microgrids-Part I: Decentralized and Hierarchical Control," *IEEE Transactions on Industrial Electronics*, vol. 60, no. 4, pp. 1254–1262, 2013.

[16] X. Lu, J. M. Guerrero, K. Sun, J. C. Vasquez, R. Teodorescu, and L. Huang, "Hierarchical control of parallel AC-DC converter interfaces for hybrid microgrids," *IEEE Transactions on Smart Grid*, vol. 5, no. 2, pp. 683–692, 2014.

[17] H. Xin, R. Zhao, L. Zhang, Z. Wang, K. P. Wong, and W. Wei, "A decentralized hierarchical control structure and self-optimizing control strategy for F-P type DGs in islanded microgrids," *IEEE Transactions on Smart Grid*, vol. 7, no. 1, pp. 3–5, 2016.

[18] J. M. Guerrero, J. C. Vásquez, J. Matas, M. Castilla, and L. García de Vicuna, "Control strategy for flexible microgrid based on parallel line-interactive UPS systems," *IEEE Transactions on Industrial Electronics*, vol. 56, no. 3, pp. 726–736, 2009.

[19] J. M. Guerrero, J. C. Vasquez, J. Matas, L. G. De Vicuña, and M. Castilla, "Hierarchical control of droop-controlled AC and DC microgrids - A general approach toward standardization," *IEEE Transactions on Industrial Electronics*, vol. 58, no. 1, pp. 158–172, 2011.

[20] J. Rocabert, A. Luna, F. Blaabjerg, and I. Paper, "Control of Power Converters in AC Microgrids.pdf," *IEEE Transactions on Power Electronics*, vol. 27, no. 11, pp. 4734–4749, 2012.

[21] J. C. Vasquez, J. M. Guerrero, A. Luna, P. Rodr??guez, and R. Teodorescu, "Adaptive droop control applied to voltage-source inverters operating in grid-connected and islanded modes," *IEEE Transactions on Industrial Electronics*, vol. 56, no. 10, pp. 4088–4096, 2009.

[22] U. B. Tayab, M. A. Bin Roslan, L. J. Hwai, and M. Kashif, "A review of droop control techniques for microgrid," *Renewable and Sustainable Energy Reviews*, vol. 76, no. May 2016, pp. 717–727, 2017.

[23] T. L. Vandoorn, J. D. M. De Kooning, B. Meersman, and L. Vandevelde, "Review of primary control strategies for islanded microgrids with power-electronic interfaces," *Renewable and Sustainable Energy Reviews*, vol. 19, pp. 613–628, 2013.

[24] N. Hatziargyriou, "MICROGRIDS – Large Scale Integration of Micro-Generation to Low Voltage Grids," *Proc. CIGRE Gen. Session, Paris, France, Paper no. C6-309*, no. Lv, pp. 1–24, 2006.

[25] M. Barnes *et al.*, "Real-World MicroGrids-An Overview," *2007 IEEE International Conference on System of Systems Engineering*, pp. 1–8, 2007.

[26] A. G. Madureira and J. A. Peças Lopes, "Coordinated voltage support in distribution networks with distributed generation and microgrids," *IET Renewable Power Generation*, vol. 3, no. 4, p. 439, 2009.

[27] J. M. Guerrero, L. Hang, and J. Uceda, "Control of Distributed Uninterruptible Power Supply Systems," *{IEEE} Trans. Ind. Electron.*, vol. 55, no. 8, pp. 2845–2859, 2008.

[28] M. Aamir, K. Ahmed Kalwar, and S. Mekhilef, "Review: Uninterruptible Power Supply (UPS) system," *Renewable and Sustainable Energy Reviews*, vol. 58, pp. 1395–1410, 2016.

[29] G. Willmann, D. F. Coutinho, L. F. A. Pereira, and F. B. Líbano, "Multiple-Loop H-Infinity Control Design for Uninterruptible Power Supplies," *IEEE Transactions on Industrial Electronics*, vol. 54, no. 3, pp. 1591–1602, 2007.

[30] P. Mattavelli, "An improved deadbeat control for UPS using disturbance observers," *IEEE Transactions on Industrial Electronics*, vol. 52, no. 1, pp. 206–212, 2005.

[31] B. Tamyurek, "A high-performance SPWM controller for three-phase UPS systems operating under highly nonlinear loads," *IEEE Transactions on Power Electronics*, vol. 28, no. 8, pp. 3689–3701, 2013.

[32] M. A. Hassan and M. A. Abido, "Optimal design of microgrids in autonomous and grid-connected modes using particle swarm optimization," *IEEE Transactions on Power Electronics*, vol. 26, no. 3, pp. 755–769, 2011.

[33] M. Ramezani, S. Li, and S. Golestan, "Analysis and controller design for stand-alone VSIs in synchronous reference frame," *IET Power Electronics*, vol. 10, no. 9, pp. 1003–1012, 2017.

[34] C. Rech, H. Pinheiro, H. A. Grundling, H. L. Hey, and J. R. Pinheiro, "A modified discrete control law for UPS applications," *IEEE Transactions on Power Electronics*, vol. 18, no. 5, pp. 1138–1145, 2003.

[35] A. Lidozzi, C. Ji, L. Solero, P. Zanchetta, and F. Crescimbini, "Resonant-Repetitive Combined Control for Stand-Alone Power Supply Units," *IEEE Transactions on Industry Applications*, vol. 51, no. 6, pp. 4653–4663, 2015.

[36] M. Niroomand and H. R. Karshenas, "Analysis and Design of a Series–Parallel Uninterruptible Power Supply with an Improved Control Strategy for Seamless Transition," *Electric Power Components and Systems*, vol. 45, no. 1, pp. 22–33, 2017.

[37] N. M. Abdel-Rahim and J. E. Quaicoe, "Analysis and design of a multiple feedback loop control strategy for single-phase voltage-source UPS inverters," *IEEE Transactions on Power Electronics*, vol. 11, no. 4, pp. 532–541, 1996.

[38]   G. Escobar, A. A. Valdez, J. Leyva-Ramos, and P. Mattavelli, "Repetitive-based controller for a UPS inverter to compensate unbalance and harmonic distortion," *IEEE Transactions on Industrial Electronics*, vol. 54, no. 1, pp. 504–510, 2007.

[39]   S. Jiang, D. Cao, Y. Li, J. Liu, and F. Z. Peng, "Low-THD, fast-transient, and cost-effective synchronous-frame repetitive controller for three-phase UPS inverters," *IEEE Transactions on Power Electronics*, vol. 27, no. 6, pp. 2994–3005, 2012.

[40]   S. Yang, P. Wang, Y. Tang, and L. Zhang, "Explicit phase lead filter design in repetitive control for voltage harmonic mitigation of VSI-based islanded Microgrids," *IEEE Transactions on Industrial Electronics*, vol. 64, no. 1, pp. 817–826, 2017.

[41]   T. L. Tai and J. S. Chen, "UPS inverter design using discrete-time sliding-mode control scheme," *IEEE Transactions on Industrial Electronics*, vol. 49, no. 1, pp. 67–75, 2002.

[42]   M. Pichan and H. Rastegar, "Sliding-Mode Control of Four-Leg Inverter With Fixed Switching Frequency for Uninterruptible Power Supply Applications," *IEEE Transactions on Industrial Electronics*, vol. 64, no. 8, pp. 6805–6814, 2017.

[43]   M. Dai, M. N. Marwali, J. W. Jung, and A. Keyhani, "A three-phase four-wire inverter control technique for a single distributed generation unit in Island mode," *IEEE Transactions on Power Electronics*, vol. 23, no. 1, pp. 322–331, 2008.

[44]   H. A. Grundling, E. G. Carati, and J. R. Pinheiro, "A robust model reference adaptive controller for UPS applications," *Proceedings of the IECON'97 23rd International Conference on Industrial Electronics, Control, and Instrumentation (Cat. No.97CH36066)*, vol. 2, pp. 901–905, 1997.

[45]   M. Aamir, K. A. Kalwar, and S. Mekhilef, "Proportional-Resonant and Slide Mode Control for Single-Phase UPS Inverter," *Electric Power Components and Systems*, vol. 45, no. 1, pp. 11–21, 2017.

[46]   P. Cortés, G. Ortiz, J. I. Yuz, J. Rodríguez, S. Vazquez, and L. G. Franquelo, "Model predictive control of an inverter with output LC filter for UPS applications," *IEEE Transactions on Industrial Electronics*, vol. 56, no. 6, pp. 1875–1883, 2009.

[47]   M. Nauman and A. Hasan, "Efficient implicit model-predictive control of a three-phase inverter with an output LC filter," *IEEE Transactions on Power Electronics*, vol. 31, no. 9, pp. 6075–6078, 2016.

[48]   S. Vazquez, J. Rodriguez, M. Rivera, L. G. Franquelo, and M. Norambuena, "Model Predictive Control for Power Converters and Drives: Advances and Trends," *IEEE Transactions on Industrial Electronics*, vol. 64, no. 2, pp. 935–947, 2017.

[49]   J. Rodriguez *et al.*, "State of the Art of Finite Control Set Model Predictive Control in Power Electronics," *IEEE Transactions on Industrial Informatics*, vol. 9, no. 2, pp. 1003–1016, 2013.

[50] J. S. Lim, C. Park, J. Han, and Y. Il Lee, "Robust Tracking Control of a Three-Phase DC-AC Inverter for UPS Applications," *Industrial Electronics, IEEE Transactions on*, vol. 61, no. 8, pp. 4142–4151, 2014.

[51] A. H. Syed and M. a. Abido, "New robust controller design for voltage source inverters in microgrids," *22nd Mediterranean Conference on Control and Automation*, pp. 734–739, 2014.

[52] E. K. Kim, F. Mwasilu, H. H. Choi, and J. W. Jung, "An Observer-Based Optimal Voltage Control Scheme for Three-Phase UPS Systems," *IEEE Transactions on Industrial Electronics*, vol. 62, no. 4, pp. 2073–2081, 2015.

[53] F. Blaabjerg, R. Teodorescu, M. Liserre, and A. V. Timbus, "Overview of control and grid synchronization for distributed power generation systems," *IEEE Transactions on Industrial Electronics*, vol. 53, no. 5, pp. 1398–1409, 2006.

[54] M. Liserre and F. Blaabjerg, "Reactive Power Control for Improving Wind Turbine System Behavior Under Grid Faults," *IEEE Transactions on Power Electronics*, vol. 24, no. 7, pp. 1798–1801, 2009.

[55] A. Timbus, M. Liserre, R. Teodorescu, P. Rodriguez, and F. Blaabjerg, "Evaluation of Current Controllers for Distributed Power Generation Systems," *Power Electronics, IEEE Transactions on*, vol. 24, no. 3, pp. 654–664, 2009.

[56] S. Test, I. Language, and L. Specification, "IEEE Standard for Interconnecting Distributed Resources with Electric Power Systems," *Electronics*, no. March. 2003.

[57] I. S. 1547-2003, "IEEE Standard for Interconnecting Distributed Resources with Electric Power Systems Amendment," *IEEE*, vol. 2014. pp. 1–16, 2008.

[58] M. Tsili and S. Papathanassiou, "A review of grid code technical requirements for wind farms," *IET Renewable Power Generation*, vol. 3, no. 3, p. 308, 2009.

[59] P. . Rodriguez, a. V. Timbus, R. . Teodorescu, M. . Liserre, and F. . Blaabjerg, "Flexible Active Power Control of Distributed Power Generation Systems During Grid Faults," *IEEE Transactions on Industrial Electronics*, vol. 54, no. 5, pp. 2583–2592, 2007.

[60] I. Vechiu, O. Curea, A. Llaria, and H. Camblong, "Control of power converters for microgrids," *COMPEL: The International Journal for Computation and Mathematics in Electrical and Electronic Engineering*, vol. 30, no. 1, pp. 300–309, 2011.

[61] Z. Yao, L. Xiao, and J. M. Guerrero, "Improved control strategy for the three-phase grid-connected inverter," *IET Renewable Power Generation*, vol. 9, no. 3, pp. 587–592, 2015.

[62] I. J. Gabe, F. Montagner, and H. Pinheiro, "Design and Implementation of a Robust Current Controller for VSI Connected to the Grid Through an LCL Filter," *IEEE Transactions on Power Electronics*, vol. 24, no. 6, pp. 1444–1452, 2009.

[63] M. Liserre, F. Blaabjerg, and S. Hansen, "Design and Control of an LCL -Filter-Based Three-Phase Active Rectifier," *IEEE Transactions on Industry Applications*, vol. 41, no. 5, pp. 1281–1291, 2005.

[64] Z. Ye, G. Sinha, and X. Yuan, "Output Filter Design for a Grid-interconnected Three-phase Inverter," in *Power Electronics Specialist Conference, 2003. PESC '03. 2003 IEEE 34th Annual*, 2003, pp. 779–784 vol.2.

[65] S. Eren, A. Bakhshai, and P. Jain, "Control of grid-connected voltage source inverter with LCL filter," in *2012 Twenty-Seventh Annual IEEE Applied Power Electronics Conference and Exposition (APEC)*, 2012, pp. 1516–1520.

[66] J. Xu, S. Member, S. Xie, and T. Tang, "Active Damping-Based Control for Grid-Connected LCL -Filtered Inverter With Injected Grid Current Feedback Only," *IEEE Transactions on Industrial Electronics*, vol. 61, no. 9, pp. 4746–4758, 2014.

[67] W. Wu, Y. Liu, Y. He, H. S. H. Chung, M. Liserre, and F. Blaabjerg, "Damping Methods for Resonances Caused by LCL-Filter-Based Current-Controlled Grid-Tied Power Inverters: An Overview," *IEEE Transactions on Industrial Electronics*, vol. 64, no. 9, pp. 7402–7413, 2017.

[68] B. Bahrani, S. Member, S. Kenzelmann, S. Member, and A. Rufer, "Multivariable-PI-Based dq Current Control of Voltage Source Converters With Superior Axis," *IEEE Transactions on Industrial Electronics*, vol. 58, no. 7, pp. 3016–3026, 2011.

[69] B. Bahrani, S. Member, A. Karimi, B. Rey, and A. Rufer, "Decoupled dq -Current Control of Grid-Tied Voltage Source Converters Using Nonparametric Models," *IEEE Transactions on Industrial Electronics*, vol. 60, no. 4, pp. 1356–1366, 2013.

[70] J. Dannehl, F. W. Fuchs, and P. B. Thøgersen, "PI state space current control of grid-connected PWM converters with LCL filters," *IEEE Transactions on Power Electronics*, vol. 25, no. 9, pp. 2320–2330, 2010.

[71] J. Jiao, J. Y. Hung, and R. M. Nelms, "State feedback control for single-phase grid-connected inverter under weak grid," in *2017 IEEE 26th International Symposium on Industrial Electronics (ISIE)*, 2017, pp. 879–885.

[72] Y. Liu *et al.*, "An Efficient and Robust Hybrid Damper for LCL - or LLCL -Based Grid-Tied Inverter With Strong Grid-Side Harmonic Voltage Effect Rejection," *IEEE Transactions on Industrial Electronics*, vol. 63, no. 2, pp. 926–936, 2016.

[73] L. A. MacCari *et al.*, "LMI-based control for grid-connected converters with LCL filters under uncertain parameters," *IEEE Transactions on Power Electronics*, vol. 29, no. 7, pp. 3776–3785, 2014.

[74] L. A. Maccari, H. Pinheiro, R. C. L. F. Oliveira, and e. V. F. Montagner, "Robust pole location with experimental validation for three-phase grid-connected converters," *Control Engineering Practice*, vol. 59, no. November 2016, pp. 16–26, 2017.

[75] N.-B. Lai and K.-H. Kim, "Robust Control Scheme for Three-phase Grid-connected Inverters with LCL-filter under Unbalanced and Distorted Grid Conditions," *IEEE Transactions on Energy Conversion*, vol. PP, no. 99, pp. 1–1, 2017.

[76] J. Perez, S. Cobreces, R. Grino, and F. J. R. Sanchez, "H∞current controller for input admittance shaping of VSC-based grid applications," *IEEE Transactions on Power Electronics*, vol. 32, no. 4, pp. 3180–3191, 2017.

[77] B. Wang, Y. Xu, Z. Shen, J. Zou, C. Li, and H. Liu, "Current Control of Grid-Connected Inverter with LCL Filter Based on Extended-State Observer Estimations Using Single Sensor and Achieving Improved Robust Observation Dynamics," *IEEE Transactions on Industrial Electronics*, vol. 64, no. 7, pp. 5428–5439, 2017.

[78] M. Sadabadi, H. Aboutaleb, H. Karimi, and A. Karimi, "A Robust Active Damping Control Strategy for," *IEEE Transactions on Industrial Electronics*, vol. 64, no. 10, pp. 8055–8065, 2017.

[79] Y. W. Li, D. M. Vilathgamuwa, and P. C. Loh, "Robust control scheme for a microgrid with PFC capacitor connected," *IEEE Transactions on Industry Applications*, vol. 43, no. 5, pp. 1172–1182, 2007.

[80] A. H. Syed and M. A. Abido, "New enhanced performance robust control design scheme for grid-connected VSI," *Control Engineering Practice*, vol. 53, pp. 92–108, 2016.

[81] A. H. Syed and M. A. Abido, "A novel strategy to design enhanced performance robust controller for standalone VSI," *Journal of the Franklin Institute*, vol. 354, no. 5, pp. 2269–2294, 2016.

[82] G. Jackson, U. D. Annakkage, A. M. Gole, D. Lowe, and M. P. Mcshane, "A Real-Time Platform for Teaching Power System Control Design," pp. 1–5.

[83] J. Lofberg, "YALMIP : a toolbox for modeling and optimization in MATLAB," *2004 IEEE International Conference on Robotics and Automation (IEEE Cat. No.04CH37508)*, pp. 284–289, 2004.

[84] J. W. Jung, M. Dai, and A. Keyhani, "Optimal control of three-phase PWM inverter for UPS systems," *2004 IEEE 35th Annual Power Electronics Specialists Conference (IEEE Cat. No.04CH37551)*, pp. 2054–2059, 2004.

[85] E. Ostertag, "Linear Matrix Inequalities," in *Mono- and Multivariable Control and Estimation*, 2011, pp. 267–290.

[86] A. H. Syed, M. A. Abido, and R. Kennel, "Improved performance of intelligent robust controller for grid-connected VSI," in *In Power Electronics and Applications (EPE'16 ECCE Europe), 2016 18th European Conference on*, pp. 1–9.

Vitae

Name   :Wasiu Olaoti Sulaimon

Nationality   :Nigerian

Date of Birth   :2/26/1986

Email   :sulaimonwasiu13@gmail.com

Address   :27 Kekereowo Street, Mushin, Lagos, Nigeria

Academic Background   :Bachelor of Science Electrical Electronics Engineering

University of Lagos, Akoko Lagos, Nigeria.